INFLUENCE OF ORIFICE PLATE SHAPE ON CONDENSER UNIT EFFECTIVENESS

by

Stephen Patrick Kuluris

A thesis submitted in partial fulfillment
of the requirements for the degree

of

Master of Science

in

Mechanical Engineering

MONTANA STATE UNIVERSITY
Bozeman, Montana

April 2018

©COPYRIGHT

by

Stephen Patrick Kuluris

2018

All Rights Reserved

TABLE OF CONTENTS

1. INTRODUCTION 1

2. BACKGROUND 5

HVAC 5
Refrigeration Cycle 5
Condenser Unit 9
Heat Exchangers. 9
Fans. 11
Orifice Plate. 13
Research Objective 15
Computational Fluid Dynamics 15
Usage in Industry 18
Visualization and Analysis 19
CFD Geometry Simplifications 24
Error and Limitations 25
Data Analysis 26

3. EXPERIMENTAL METHODOLOGY 31

Porosity Data 31
Velocity Data 32

4. COMPUTATIONAL FLUID DYNAMICS METHODOLOGY 36

Model Simplifications 36
Geometry 36
Inlet 36
Outlet 38
Model Parameters 38
Simulation 38
Data Collection 39
Model Validation 41
Redesign 42
Current Orifice 42
Orifice Inlet 44
Orifice Outlet 46

TABLE OF CONTENTS – CONTINUED

5. RESULTS 48

CFD Validation 48
Redesign Analysis 54
Inlet Curvature 54
Outlet Curvature 67
Combined Orifice 75

6. CONCLUSION 78

REFERENCES CITED 81

LIST OF TABLES

Table Page

4.1 Physics parameters 39
4.2 Simulation parameters 39
5.1 Simulation parameters 59
5.2 Results parameters 77

LIST OF FIGURES

Figure Page

2.1 Simplified refrigeration cycle 6

2.2 T-s and p-h diagrams with saturation curve for an ideal cycle where C is a constant [11] 7

2.3 Micro-channel coil and micro-channel bends [26] 10

2.4 A-frame unit with blow-through configuration [27] 11

2.5 Residential unit with horizontal inflow and vertical outflow [20] 12

2.6 Axial fan with airflow parallel to rotation axis 12

2.7 Centrifugal fan with airflow radial to rotation axis [25] 13

2.8 General example of fan curve [25] 14

2.9 Fan casing surrounding the fan 15

2.10 Condenser unit with angled refrigeration coil and axial fan 16

2.11 Contour plot of velocity colored by magnitude 20

2.12 Vector plot with line convolution integral of velocity colored by magnitude 21

2.13 Streamlines tracing flow from inlet to outlet of the fluid domain 22

2.14 Isosurface of velocity ranging from 6-12m/s 28

2.15 Line and grid probes placed within the fluid domain 29

2.16 XY plot of velocity distribution downstream of a condenser unit fan 30

3.1 Experimental pressure drop and velocity data with quadratic fit 32

3.2 Partially shielded TSI 9535 air velocity meter probe 33

3.3 Three vertically placed horizontal velocity traverses 34

3.4 Three vertically placed horizontal velocity traverses 35

3.5 Experimental setup for condenser unit 35

4.1 Simplified geometry of condenser unit 37

LIST OF FIGURES – CONTINUED

Figure Page

4.2 Line probe and grid used for simulation data collection 40

4.3 Current geometry sketch..... 43

4.4 Current geometry with fan placement..... 43

4.5 Example inlet geometry sketch..... 45

4.6 Example inlet geometry with fan placement..... 45

4.7 Example outlet geometry sketch..... 47

4.8 Example outlet geometry with fan placement..... 47

5.1 Velocity profile for center-to-back traverse magnitude (top) and z-component (bottom) 50

5.2 Velocity vector scene with velocity deficit due to motor. 51

5.3 Z-component velocity profile for center-to-side traverse..... 52

5.4 Z-component velocity profile for center-to-front traverse 52

5.5 Z-component velocity profile for center-to-back traverse at vertical height of 0.127m (left) and 0.179m (right)..... 53

5.6 Z-component velocity profile for center-to-side traverse at vertical height of 0.127m (left) and 0.179m (right)..... 53

5.7 Z-component velocity profile for center-to-front traverse at vertical height of 0.127m (left) and 0.179m (right)..... 53

5.8 Constant curvature case with increasing width and height 54

5.9 Velocity vector plot of 0.005m radius (left) and 0.045m radius (right) 56

5.10 Changing inlet height with a constant 0.045m width 56

5.11 Velocity vector plot of 0.005m height (left) and 0.085m height (right) 57

5.12 RSM surface plot with VFR response variable 58

5.13 Velocity vector plot of 0.005m width (left) and 0.045m width (right) with same 0.085m height 59

LIST OF FIGURES – CONTINUED

Figure Page

5.14 RSM surface plot with fan efficiency response variable 60

5.15 Velocity vector plot of original orifice (left) and VFR optimal orifice (right) 61

5.16 Velocity vector plot of original orifice (left) and fan efficiency optimal orifice (right) 62

5.17 Front view of turbulent kinetic energy generation 62

5.18 Isosurface of turbulent kinetic energy entering fan area 63

5.19 Surface plot of velocity distribution at the coil face 64

5.20 Magnitude comparison of velocity distribution at the face of the coil 65

5.21 Normalized velocity distribution at the face of the coil for original orifice (top) and most efficient orifice (bottom) 66

5.22 Pressure distribution upstream of fan driving flow velocity 67

5.23 VFR response with increasing height for given width 67

5.24 VFR response with increasing height for given width 68

5.25 Efficiency response with increasing height for given width 69

5.26 Efficiency distribution for curvature of outlet 69

5.27 Interpolated fan efficiency response distribution with maximum fan efficiency trend 70

5.28 Pressure of original orifice (left) and most efficient outlet orifice (right) 71

5.29 Vorticity of original orifice (left) and most efficient outlet orifice (right) 72

5.30 Pressure of most efficient orifice (left) and orifice with increased curvature beyond optimal (right) 72

5.31 Magnitude comparison of velocity distribution at the face of the coil 73

LIST OF FIGURES – CONTINUED

Figure Page

5.32 Normalized velocity distribution at the face of the coil for original orifice (top) and most efficient orifice (bottom) 74

5.33 Velocity vector plot at inlet of combined orifice 76

5.34 Vorticity at outlet of combined orifice 76

ABSTRACT

In both residential and commercial buildings, heating, ventilation and air-conditioning (HVAC) is the largest consumer of energy. The HVAC industry works to consistently reduce their energy consumption in order to lower consumer costs and to stay competitive in the field. Therefore, improving fan efficiency of any component in an HVAC system is beneficial. A major part of the industry is to use the vapor-compression refrigeration cycle to cool buildings and an essential component of the cycle is the condenser unit. Axial fans are commonly used to move air through and cool the heated refrigerant coil. Improving axial fan performance by redesigning the casing that surrounds the fan, known as an orifice plate, is suspected to lead to a more productive condenser unit. Changing the geometry can increase performance by reducing turbulence generation both upstream and downstream of the fan, which is thought to be a major contributor to loss in fan fan efficiency. Manufacturing many different geometries in a design process to find an improved orifice plate is time-consuming and expensive. With advances in computer technologies, computational fluid dynamics (CFD) has become a low-cost alternative to iterative, physical prototyping. This work uses CFD in the design process of an orifice plate, to characterize and analyze the effects of different geometries. Fan fan efficiency and volume flow rate characterize the performance of the design, and turbulence, vorticity, and pressure visualization provides further information about the effects of design changes. The orifice geometry upstream and downstream of the fan were changed independently, and then both regions were combined into a single design. Results show that the flow upstream and downstream are affected in different ways, and contribute to overall fan efficiency through different mechanics. An improvement to the inlet region produced an fan efficiency increase of 4.8%, and the addition of an outlet region increases fan efficiency by 9.8%. The combined change in the orifice resulted in an overall increase in fan efficiency by 15.85% over the original design.

CHAPTER ONE

INTRODUCTION

In 2016, the residential and commercial building sectors accounted for 40% of the total energy used in the United States [1]. Reducing energy use in this sector presents an opportunity for significant cost savings, and a reduction in carbon emissions. This has led to an increase in energy-efficient building designs and energy-efficient technologies utilized in the design. Within the building sector, heating, ventilation and air-conditioning (HVAC) is the largest consumer of energy, and accounts for 48% and 44% of residential and commercial buildings' energy use, respectively [2, 3]. With a significant portion of energy focused on these systems, HVAC components and processes can have substantial energy savings and cost reductions within residential and commercial buildings. Researchers have looked at utilizing more efficient compressors in the refrigeration cycle, reducing energy use in the dehumidification process, and using control strategies for ventilation and air movement throughout buildings [4–7]. Many other HVAC elements hold the potential to decrease operating costs and energy use, including the condenser unit used in cooling and heating processes.

Heating and cooling air that is distributed throughout a building is fundamental to the HVAC industry. This discipline of HVAC allows people to live and work in what, otherwise, would be extremely cold or hot conditions. Beyond allowing cities in these types of environments to grow, heating and cooling a work place has shown to have major effects on productivity [8]. A vital element in achieving heating and cooling is the condenser unit; a heat exchanger made up of multiple

components. A common condenser unit uses a fan to move air over a coil that contains a refrigerant. By passing air through the coil, energy is exchanged between the air and the refrigerant. The effectiveness of the condenser unit as a heat exchanger depends on the amount of energy that is exchanged between the two fluids. The energy exchange is dependent on both velocities and the flow distribution of the air over the coil [9, 10]. Therefore, better distribution of air over a coil, and an increased movement of air through the coil can achieve better efficiencies. The placement of the fan within the condenser unit, both orientation and distance from the coil, can improve the distribution and efficiency [11]. The fan itself can also have great effects on the performance, by increasing volume flow through the coil. This can be improved by changing blade type such as forward or backward swept, by varying the number of blades used, or by changing elements of the blade, such as tip shape [12–14].

Other efficiency increases can come from changing the operating environment of the fan, such as altering the fan housing, which surrounds the fan and allows flow to only pass through the fan area. The size and shape of this housing, and the position of the fan relative to it, impact fan efficiency and noise production. The clearance between the tip of the blade and the housing has shown to have a significant effect on the efficiency and noise produced by axial flow fans. Increased tip clearance consistently results in a rise in sound pressure levels and decreases in the efficiency of the fan [15, 16]. This is due to more flow passing around the fan through the clearance, instead of through the fan area, decreasing volumetric flow and efficiency, as well as allowing vortices to develop off the tip of the blade, increasing aerodynamic noise. Guedel et al. have shown that the addition of a contoured inlet bell-mouth increases performance of fans and that the length of the inlet to the fan effects fan performance [17]. The initial radius that the contoured inlet has, can also be optimized for best performance. In general, the larger the radius becomes the

better the performance, due to the increased intake area forcing the flow through the fan; however, radii are limited due to the unit size, and how much space the fan and housing are able to occupy [18]. Other researchers have looked at addressing multiple fan casing parameters in total redesigns for a given fan. Ren, et al, optimized the length of a fan casing, and the placement of the fan within the casing. The results showed increasing the casing length had an increase in total flow rate as it closely resembled ducted flow, and vortex shedding was decreased. However, casing length reached a maximum dimension where further increases had little effect on increasing flow rate [19]. Wang et al, investigated how fan performance is influenced by the clearance between an axial fan and the surrounding housing [20]. The testing showed decreasing the clearance weakened tip vortices, which are a significant driver of performance loss and increased noise.

Engineers and designers formerly relied on physical prototyping and testing in order to optimize parts and whole systems. This can be an expensive and time consuming process as it could require purchasing of new physical parts, and labor to build a number of prototypes. Furthermore, physical data and visualization can lack detail when the system becomes overly complex. This could lead to false conclusions that influence final design. With the introduction of computers and numerical modeling programs, part of this prototyping and design work can be done using numerical methods. This allows designers to iterate over multiple designs before potentially prototyping one final design. Within numerical method programs, data analysis and visualization is often much easier to study in detail, leading to better understanding of the system, which is necessary to properly design parts or systems.

When designs are influenced by fluid interactions, computational fluid dynamics (CFD) can help reduce cost and time spent on the iterative design process. Using CFD, computer simulations can be applied to different designs or environmental

conditions quicker than physically prototyping or changing particular parameters of a test. Recent years have seen an increase in CFD use in the HVAC industry, from ventilation movement to energy recovery devices [21, 22]. However, using CFD throughout the design process of a part or system is still relatively new to the industry. Increasing CFD use in the HVAC industry could lead to decreased costs and energy savings for both manufacturer and the end user due to more efficient designs.

This research aims to employ CFD and experimental work in the design process of an orifice plate surrounding an axial fan within a condenser unit. The objectives of a new design are to increase efficiency of the fan, reduce noise of the fan and distribute airflow over the coil more effectively. By reaching these objectives, the condenser unit's performance will increase as a whole, leading to reduced costs and energy at the consumer level.

CHAPTER TWO

BACKGROUND

This section explains the systems and components necessary for heating and cooling. Specifically, the refrigeration cycle is discussed as it is necessary for heating and cooling to occur. Heat exchangers and fans are then introduced as these are used to complete the necessary refrigeration cycle. CFD is also introduced, including the methods it uses and the limitations it has when modeling fluid flow. Additionally, data analysis techniques are discussed that are utilized in this research.

HVAC

HVAC is a system that helps condition the indoor environment of a building. Differences in building size, location and intended use, leads to differing HVAC systems, including variations in size, shape, and the necessary components. An obvious goal of these systems is to heat and cool the air inside the building. Heating and cooling are important processes, as indoor temperature is essential for comfortable working and living conditions within a building.

Refrigeration Cycle

The vapor-compression refrigeration cycle is a thermodynamic process that makes heating and cooling possible. A simplified refrigeration cycle is shown in Figure 2.1, where $\dot{Q}_{out}$ is the heat transfer rate out of the refrigerant, $\dot{Q}_{in}$ is the heat transfer rate into the refrigerant and $\dot{W}_c$ is the mechanical work that goes into the compressor. Stations 1, 2, 3 and 4 correspond to locations within the refrigeration cycle. The components required for the simplified process are a compressor, condenser, expansion valve and an evaporator. Additionally, a working

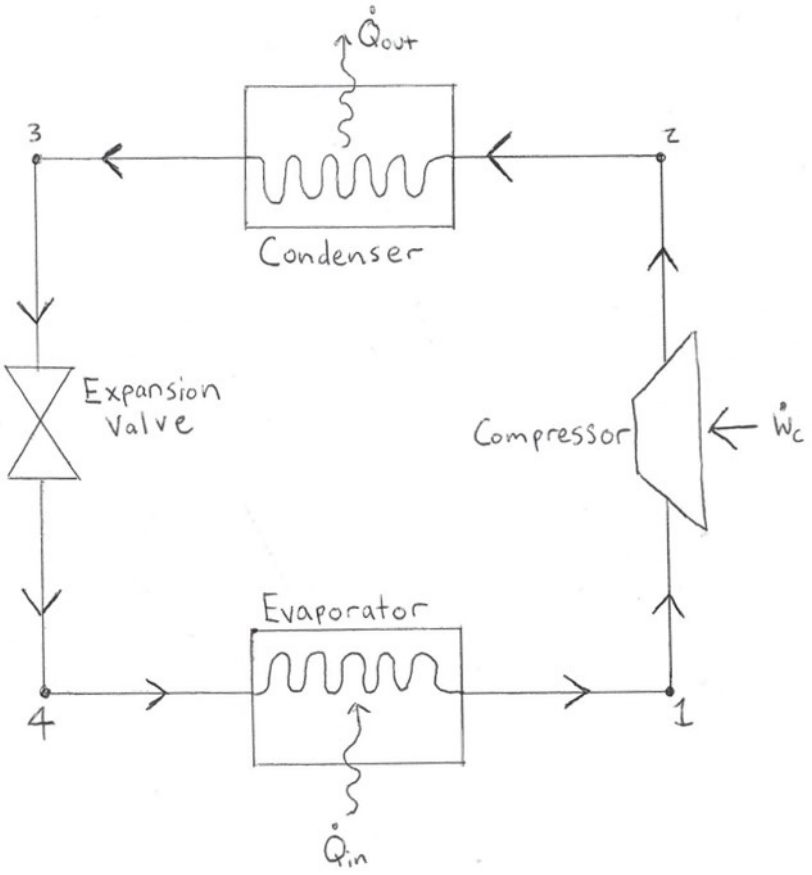

Figure 2.1: Simplified refrigeration cycle

fluid, or refrigerant, is needed to cycle through the process. A compressor and expansion valve are used to raise and lower the pressure of the refrigerant, respectively. The condenser and evaporator are heat exchangers that give up or take away energy from the refrigerant through heat transfer [23]. Refrigerants are chosen based on their thermodynamic properties, including heat of vaporization, boiling point, and necessary operating pressures in the condenser and evaporator [24]. The refrigerant operates near its boiling point, and changes phase and thermodynamic properties throughout the cycle. Two of these properties are entropy (s) in Joules per Kelvin (J/K), which measures molecular disorder, and enthalpy (h) in Joules (J), which

shows system energy and is given by

$$h = u + pv, \tag{2.1}$$

where u is internal energy, p is pressure and v is specific volume. A temperature-entropy (T-s) diagram and pressure-enthalpy (p-h) diagram, shown in Figure 2.2, track these thermodynamic changes through the refrigeration cycle. A saturation vapor curve is also shown on these diagrams, and tracks the location where phase changes occur. Increasing the pressure of the refrigerant with the compressor,

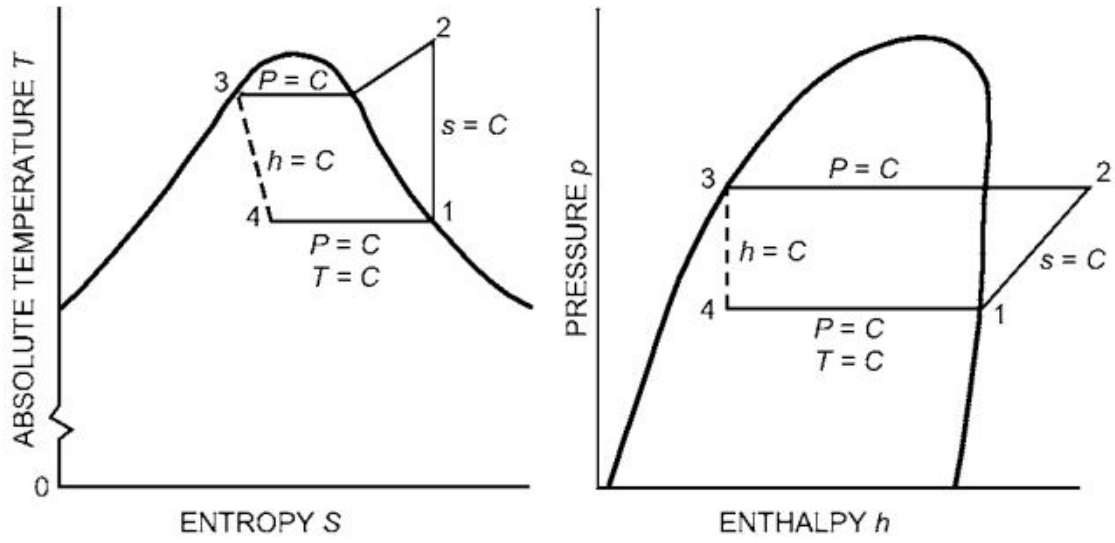

Figure 2.2: T-s and p-h diagrams with saturation curve for an ideal cycle where C is a constant [11]

raises the temperature and the refrigerant enters the condenser as a hot vapor. Similarly, decreasing the pressure of the refrigerant with the expansion valve, lowers the temperature and the refrigerant enters the evaporator as a cold liquid-vapor mixture. Passing the refrigerant through the expansion valve is a constant enthalpy process, giving $h_3 = h_4$. In the condenser, energy is released by the refrigerant,

lowering its overall enthalpy, whereas energy is absorbed in the evaporator, and its overall enthalpy is raised. The total energy released by the refrigerant is given by the enthalpy difference across the condenser as,

$$\dot{Q}_{out} = \dot{m}(h_2 - h_3) \tag{2.2}$$

where $\dot{m}$ is the mass flow rate of the refrigerant and h_2 and h_3 are the enthalpy values of the refrigerant before and after the condenser, respectively. Similarly, the total energy absorbed by the refrigerant is given by the enthalpy difference across the evaporator as,

$$\dot{Q}_{in} = \dot{m}(h_1 - h_4) \tag{2.3}$$

where h_4 and h_1 are the enthalpy values before and after the evaporator, respectively.

There are multiple parameters used to characterize the refrigeration cycle. The effectiveness of the cycle can be evaluated with the coefficient of performance (COP) as,

$$COP = \frac{\dot{Q}_{in}}{\dot{W}_c} = \frac{(h_1 - h_4)}{(h_2 - h_1)} \tag{2.4}$$

giving a ratio of useful heat transfer out and mechanical work in to the process, where the mechanical work in $\dot{W}_c$ is the power supplied to the compressor. The numerator is known as the refrigeration capacity, and shows the useful cooling load produced by the system. Since h_4 is dependent on how low h_3 is after the condenser, increasing the heat transfer rate in the condenser, $\dot{Q}_{out}$, to drive h_3 lower, would directly affect both the COP and refrigerating capacity.

The heat transfer rates of the condenser and evaporator allows for heating and cooling in a building to take place. This occurs by passing air supplied to the building over a hot coil for heating, and a cold coil for cooling. Though components and stages

can vary from system to system, the refrigeration cycle remains the main mechanism to allow heating and cooling a building to occur.

Condenser Unit

This project focuses on one section of the refrigeration cycle; the condenser. The condenser unit is a heat exchanger responsible for cooling down the refrigerant once it has left the compressor as a hot vapor. The method of heat exchange, and the configuration of the unit can change based on different requirements of the system.

Heat Exchangers. Three types of heat exchangers are commonly used for condensers; water-cooled, air-cooled and evaporative condensers that use water and air to cool a coil [25]. Four common types of water-cooled condensers are a shell-and-tube, shell-and-coil, tube-in-tube and a brazed plate. Each kind of water-cooled condenser has a different orientation, contact between the water and refrigerant and different properties. Water availability, location, costs and other variables influence the type of condenser used. Water-cooled units can be cheaper to operate than other options if a low cost water source is available.

Evaporative condensers use both water and air, by spraying a condenser coil with water, as well as consistently applying an airflow over the coil. This results in energy dissipation by both convective heat transfer from the airflow, and evaporation of the water off the coil. Since two forms of heat transfer are occurring, with both the water, and air movement, higher heat transfer rates generally result. These greater heat transfer rates require less coil surface area for the same cooling capacity as water or air-cooled units, giving more compact units for the same capacity. Evaporative condensers can also be operated at lower temperatures than air-cooled, since heat transfer is driven by wet-bulb temperature rather than dry-bulb.

Air-cooled condensers can use a number of coil designs, however, use of newer micro-channel coils is increasing due to their higher heat exchange rates (Figure 2.3). There can be a single or multiple rows of the coil, and they are cooled by passing air through the coil with either natural or forced airflow. The heat transfer out of the

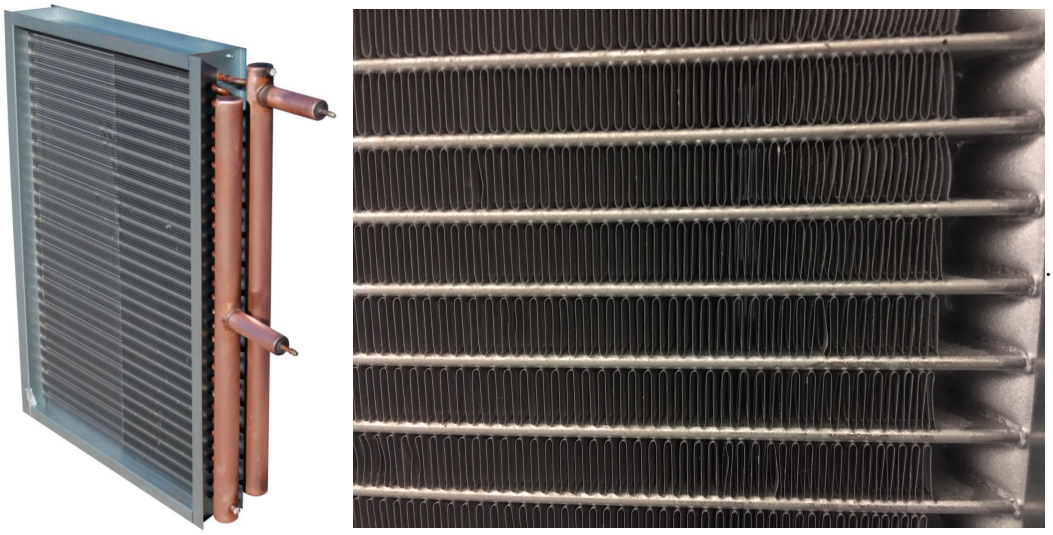

Figure 2.3: Micro-channel coil and micro-channel bends [26]

refrigerant in such an air-cooled coil can be written as,

$$\dot{Q}_{out} = UFAN\Delta T \tag{2.5}$$

where U is the heat transfer coefficient, F is a coil core surface parameter, A is the coil face area, N is the number of rows of a coil, and ΔT is the temperature difference between the refrigerant and the air stream. Alternatively, the heat transfer rate into the air is given by Equation 2.2, with mass flow rate, $\dot{m}$ given by,

$$\dot{m} = \rho AV \tag{2.6}$$

where ρ is the density of air, and V is the velocity at the coil surface. From this

equation, it is clear that higher velocities through an air-cooled condenser result in greater heat transfer, and therefore a more effective refrigeration cycle. Thus, forced airflow is a more common practice than natural convection, due to the higher velocities achieved using fans to move the air over the coil.

The setup of the forced air-cooled condenser can vary depending on the application. The fan can be placed upstream or downstream of the coil, resulting in a blow-through or draw-through configuration, respectively. An example of blow-through is shown in Figure 2.4, and a draw-through type is shown in Figure 2.5.

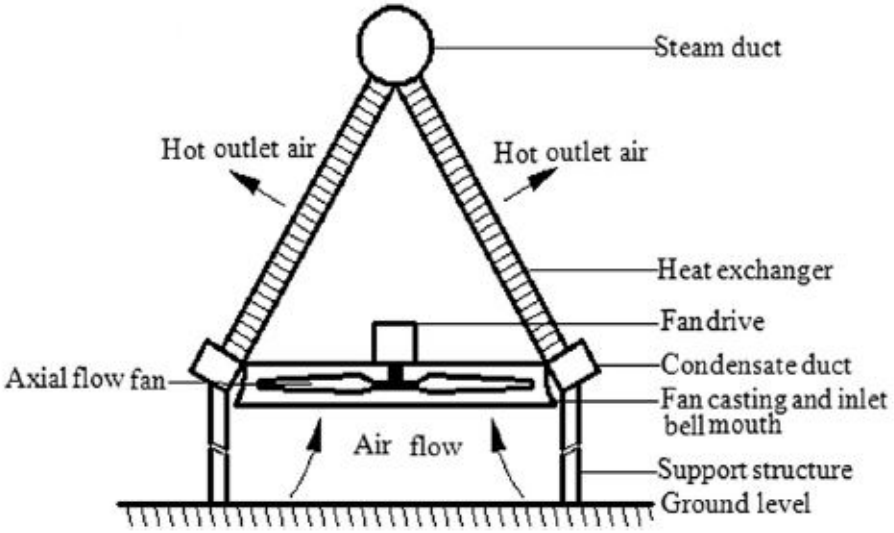

Figure 2.4: A-frame unit with blow-through configuration [27]

The orientation of the coil can also be changed depending on the system needs. A common configuration is to have the coil oriented at an angle, blowing air through the coil, and expelling air normal to the coil out the top as shown in Figure 2.4. Whereas, residential air-conditioning units, which need to be more compact, often have a vertical coil wrapping the unit, and air is drawn through the coil horizontally, and expelled vertically out the top of the unit as shown in in Figure 2.5.

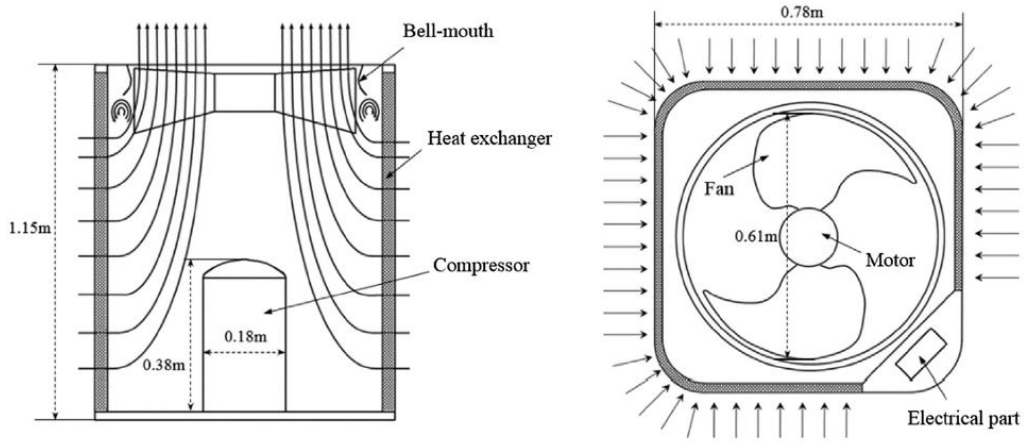

Figure 2.5: Residential unit with horizontal inflow and vertical outflow [20]

Fans. There are two types of fans commonly found in HVAC applications, known as axial and centrifugal fans. An axial fan moves air parallel to the axis of rotation (Figure 2.6), whereas a centrifugal fan moves air radially to its rotation axis (Figure 2.7) [25]. The two types are useful for different purposes given the

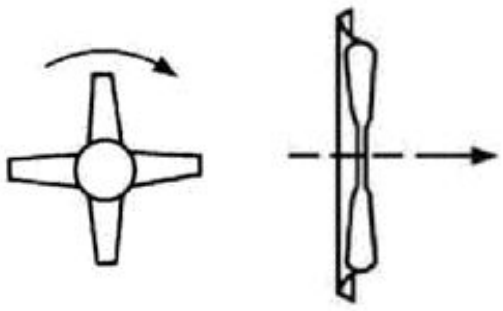

Figure 2.6: Axial fan with airflow parallel to rotation axis

characteristics of the the operating region. A centrifugal fan is more commonly found in applications that require overcoming large static pressures such as pushing air throughout a building with large ducting networks. The axial fan is more suited for applications that need large volume flow rates at low static pressure. Since blowing or drawing air through a condenser coil is often a relatively low pressure application, and

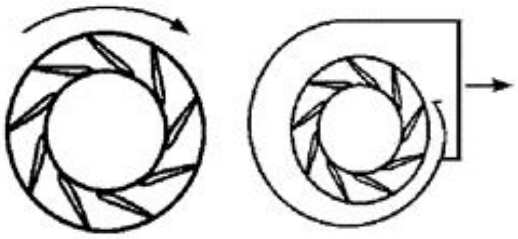

Figure 2.7: Centrifugal fan with airflow radial to rotation axis [25]

the effectiveness of a coil is strongly correlated to velocities at the coil surface, the axial fan is commonly used in condenser units. The fan efficiency is used to characterize the performance at a certain operating point, and is given by Equation 2.7 as,

$$\eta = \frac{VFR \cdot \Delta p}{W} \tag{2.7}$$

where η is the fan efficiency, VFR is the volumetric flow rate, Δp is the pressure difference across the fan, and W is the electrical power supplied to the fan.

Fan manufacturers often test fans at various operating points and develop fan curves that show how a performance changes over a range of conditions. This is often done by changing the operating pressure of the fan, and recording volumetric flow rate, pressure and power. These curves are inherent to the specific fan, and can be used to select a fan for a particular application. A selection is usually made where the pressure and volume flow rate meet the characteristics of the operating environment, and the fan efficiency is at its maximum in the operating region. An example of a fan curve is shown in Figure 2.8. Generally, there is a decrease in total pressure as the volumetric flow rate (VFR) increases, and power slowly rises as VFR increases. The fan efficiency rises from 0% until some maximum efficiency operating point before decreasing.

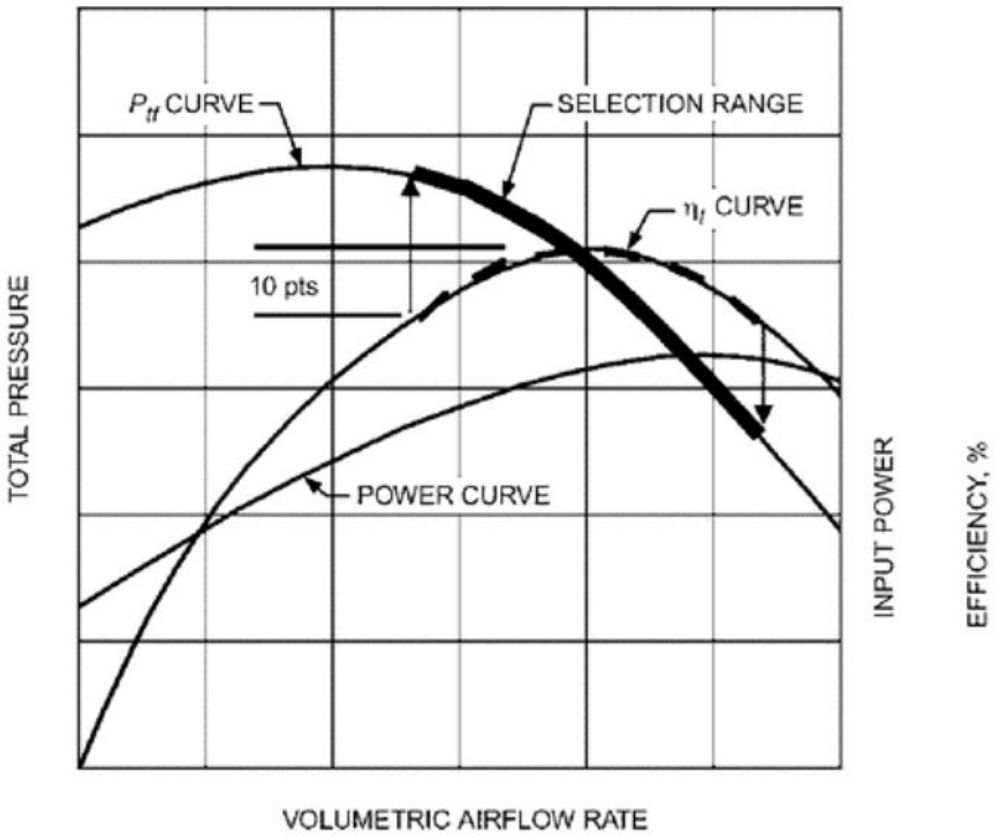

Figure 2.8: General example of fan curve [25]

Orifice Plate. Many parameters can affect the efficiency of a fan, including inflow and outflow distortions, and tip vortex shedding [15, 17, 28]. Increasing these parameters leads to lower efficiencies, as energy is used to cause flow distortions. Inflow or outflow distortions can be reduced using fixed stators, that direct the flow into or out of the fan [29]. Tip vortices can be reduced by changing the blade design by adding sweep, or by altering the geometry on the blade tip to break of the vortex [14]. Additionally, the fan casing, or orifice plate, (Figure 2.9) surrounding the fan can be used to reduce these types of distortions, and increase the efficiency of the fan.

By increasing the entrance or exit lengths, the fan casing can help straighten the flow, allowing less energy to be used in flow distortion. The inlet width of the

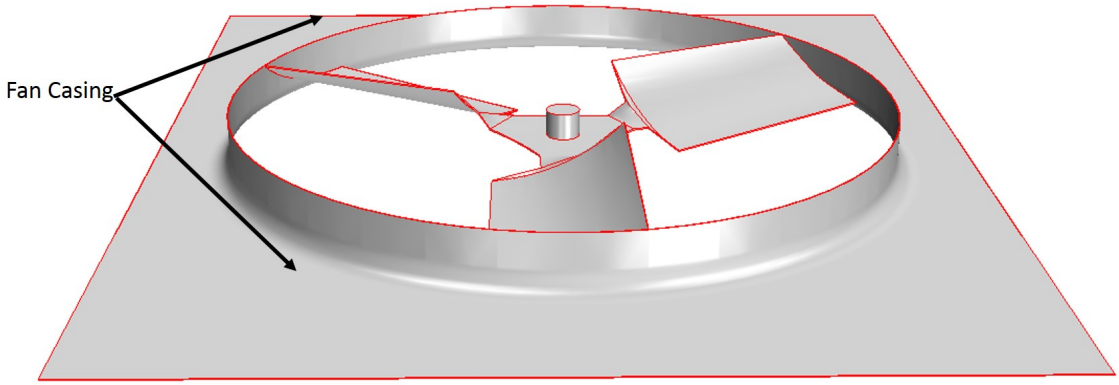

Figure 2.9: Fan casing surrounding the fan

fan casing can also increase performance by increasing the area the fan pulls air from as the width is widened, allowing higher volumetric flow rates. By reducing the gap between the fan casing and the rotors of the fan, the fan casing can also decrease tip vortex shedding. This minimizes the size of the vortex that can form and shed off of the blade tip, again, allowing less energy to be used in flow distortion.

Research Objective

The research objective for this study is to increase the effectiveness of the condenser unit by redesigning the orifice plate. A V-frame forced air-cooled condenser unit shown in Figure 2.10, is used as the experimental object. An axial fan is used to move air over the micro-channel heat exchanger, and vertically out the top of the unit. This research aims to focus on the orifice plate and its relation to fan and condenser performance through geometry changes.

Computational Fluid Dynamics

The governing equations of fluid motion, known as the Navier-Stokes equations, are a highly complex set of partial differential equations (PDE) for which there are

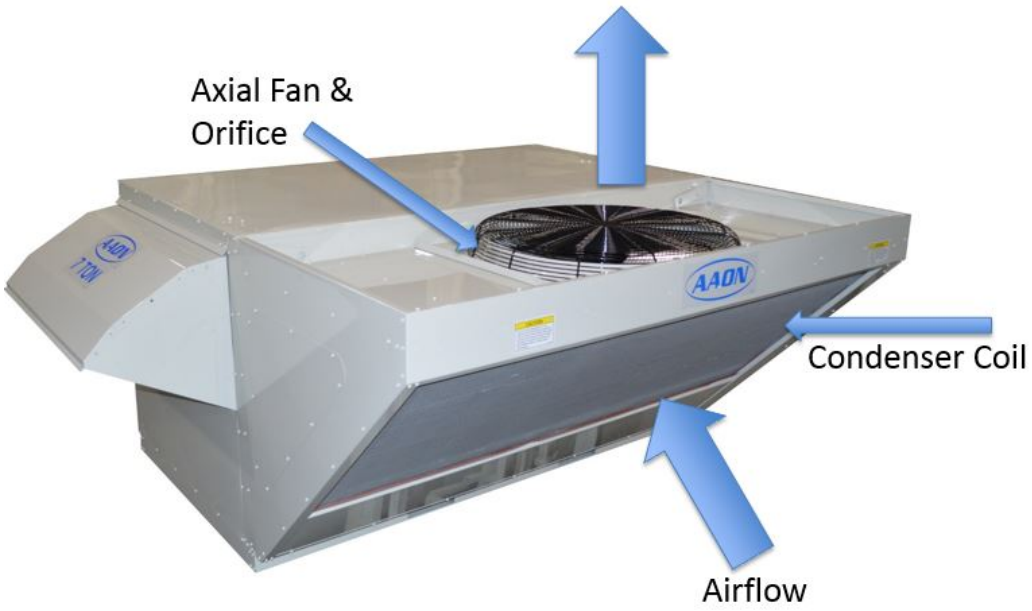

Figure 2.10: Condenser unit with angled refrigeration coil and axial fan

limited analytical solutions. Thus, computational fluid dynamics was developed as a numerical tool to study fluid motion problems by reducing the complex governing equations to a set of solvable equations. One method to solve this set of equations is by using finite difference methods (FDM), which use a Taylor-Series expansion to obtain finite difference approximations to the PDEs [30]. These approximations of the PDEs yield a set of algebraic expressions which can be solved numerically. The discretization and resulting approximation occurs on a grid that overlays the fluid region to be solved. The FDM method is often used on a grid with regular spacing, known as a structured grid, as this method is sensitive to grid spacing to maintain accuracy of the solution. When used on a structured grid, the FDM can obtain a high degree of accuracy with higher order approximations; however, conservation laws can fail if care is not taken setting up the FDM. Though structured grids can offer high accuracy, they limit the ability to model more complex geometry that cannot be represented by a typical Cartesian grid.

Another approach to solving the governing equations is known as the finite volume method (FVM) [30]. This method uses the integral form of the Navier-Stokes equations in the discretization rather than the PDE form. The discretized equations are then solved on a series of discrete continuous control volumes which make up the fluid region. This method allows for the use of non-uniform, unstructured grids since the equations are solved within the control volume and the grid merely makes up the boundaries of the control volume. A disadvantage of the FVM is that approximations greater than second order are difficult to obtain in three dimensional space [30]. However, the ability to adapt to complex geometries that are encountered in real applications, make the FVM the widely used method in many CFD commercial software packages.

Many flows that are observed in the real world contain turbulence, which is a chaotic motion of the fluid due to disturbances in the flow. The onset of these disturbances in a flow field are correlated to the non-dimensional Reynolds' number (Re) that relates inertial effects of the flow to viscous effects. Low Re values indicate a flow with relatively large viscous effects and these viscous effects tend to dampen disturbances. As Re values increase a flow becomes increasingly dominated by inertial effects and disturbances and the resulting chaotic motions tend to perpetuate. A smooth flow where disturbances are dampened are known as laminar flows, whereas a flow that perpetuates disturbances is known as a turbulent flow.

Turbulence is not captured in the governing equations, and therefore, must be dealt with in additional equations. One of the most common methods of dealing with turbulence is done by taking the time-averaged values within the flow field, and ignoring any instantaneous fluctuations. This method is known as the Reynolds Averaged Navier-Stokes (RANS). Another method is known as the Large Eddy Simulation (LES) where larger vortex structures are solved for directly, and smaller

scale structures are filtered out around the grid scale. By solving directly for large scale structures, this method is more computationally expensive than a RANS model because LES often requires a finer grid. A Detached Eddy Simulation (DES) combines both RANS and LES, by using either model depending on vortex length scales, grid sizes, and distance to solid boundaries. The most effective way of solving for turbulence is known as a Direct Numerical Simulation (DNS) that solves the flow field directly with no approximations other than the discretized method used to reduce the governing equations. Such simulations are incredibly computationally expensive, and require fine grids to solve small length scale vortices. Therefore, most applications of CFD use RANS, LES or DES.

Usage in Industry

The development of CFD and these methods as a tool for flow analysis, has lead to widespread use in many industries, such as aerospace for aircraft aerodynamics, automotive industry for modeling combustion and flow in engines, ship hydrodynamics, and for renewable energy across various technologies, including wind power [31–34]. The HVAC industry has also embraced CFD as a tool for progressing the field. LES simulations have been carried out to model natural building ventilation, CFD models have been developed to handle heat and mass transfer in energy exchangers, and CFD packages can also use post processing to model noise of HVAC equipment [35–37].

Most applications of CFD are used for design optimization, to obtain the desired flow characteristics of a particular object or system. CFD is particularly useful for this type of iterative process, because computer models of many different designs is often much faster and cheaper to produce than prototyping physical objects. This allows for many more iterations to take place in the design process than physical

prototyping, and thus, more likely that the most optimal design will be found.

When using CFD to perform such an iterative design process, it is generally expected to validate the CFD model first, based off experimental data to ensure the model appropriately captures and predicts the physics of the real world. Once a model is validated, CFD can be used to change designs, or test different environmental conditions or inputs. The model could become invalid, if there are drastic changes introduced that change the driving factors of the system. Therefore, once a final design is achieved, it is usually validated again by prototyping a final design and comparing experimental results to ensure the model is still representing the correct physics of the flow. Depending on model size, simulation run time, grid size and other factors, the entire design process can take place on a single workstation. If models increase in size or complexity, multiple work stations or high performance computers (HPC) can be used to carry out the CFD simulations.

Visualization and Analysis CFD packages offer enormous amounts of information for a simulation, and have the ability to output large amounts of data at every time step or iteration. Outputting every variable for each iteration would quickly cause memory issues on most workstations. Therefore, CFD packages often require the user to specify the type of information they would like to collect from the model, before the simulation is ran.

Flow visualization is one piece of information that can be collected in CFD, and there are a variety of ways to view the flow. One such method is with contour plots of scaler values as shown in Figure 2.11. These type of plots can help visualize flow structure and magnitudes in particular areas. Another method is using a vector scene, which helps display direction and magnitude of a parameter as shown in Figure 2.12. Streamlines are another visualization tool that trace the instantaneous tangent to

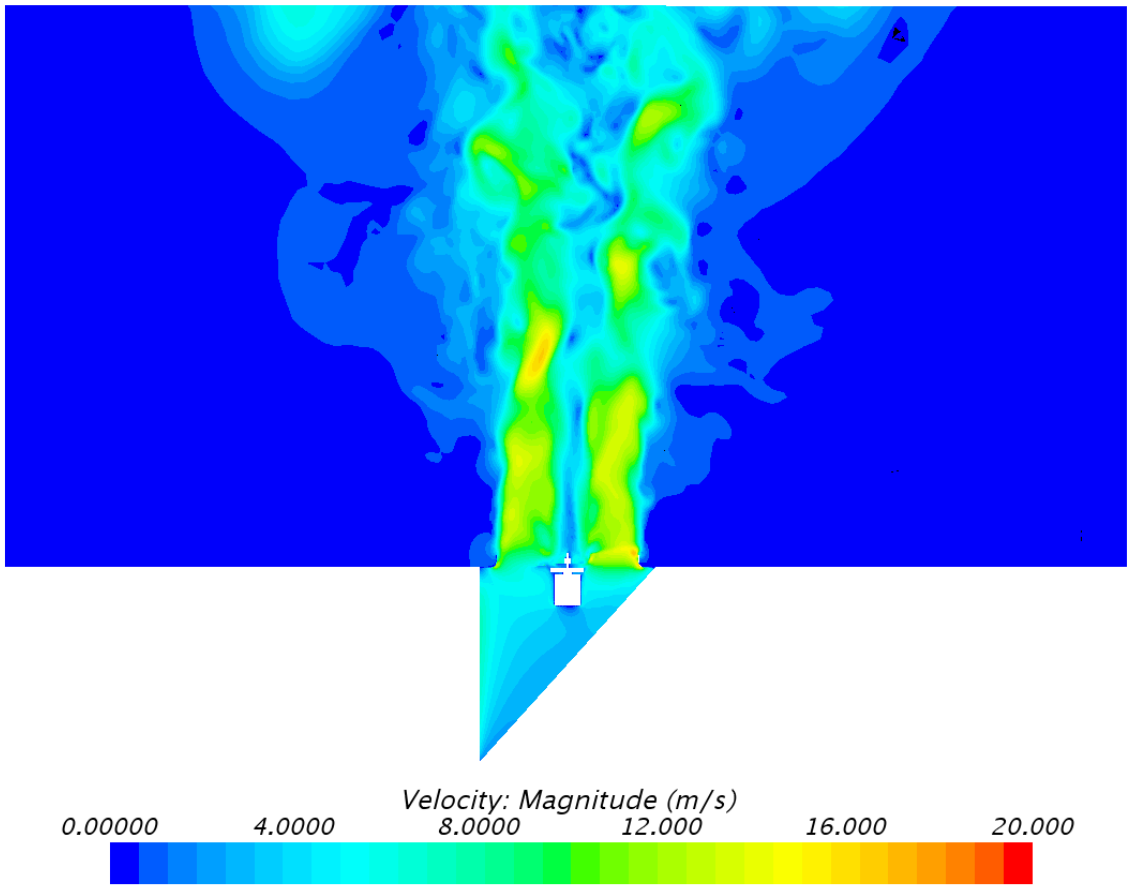

Figure 2.11: Contour plot of velocity colored by magnitude to visualize flow structure and magnitudes in particular areas

velocity through the area of interest as seen in Figure 2.13. This type of scene can help in identifying reversed flow, or turbulence and swirl locations. Isosurfaces, shown in Figure 2.14), are a surface that produces a contour surface at a specific value of a parameter. It can show a single value or a range of values, and can help outline specific areas of flow based on the value of interest.

Other ways of viewing a fluid flow profile can be done with numerical values on XY plots. The value of a particular parameter can be collected at discrete locations within the flow field using probes, as shown in Figure 2.15. Data from these probes can then be plotted to get an idea of the distribution of the values across the probe,

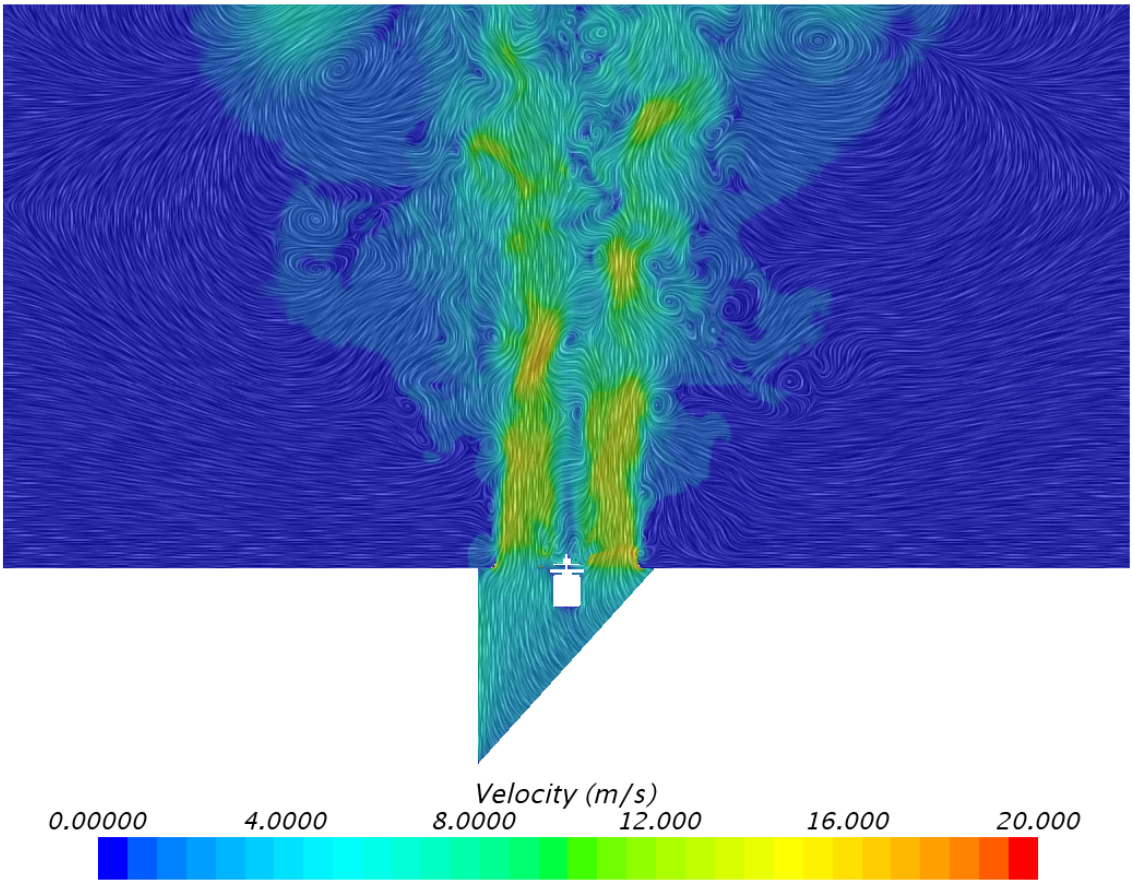

Figure 2.12: Vector plot with line convolution integral of velocity colored by magnitude used to view magnitude and direction of a parameter

as shown in Figure 2.16.

Analyzing a flow field may strictly require numerical values associated with a flow. Time histories of parameters such as: mass flow, forces or torques on solid surfaces, pressure differences across a domain, or temperatures can be collected throughout a simulation's run time.

Fluids problems can vary widely, and may require different analysis methods and parameters in order to understand the flow field. However, there are some common parameters that can be used to characterize and analyze different flow fields. Reynolds number, velocity, and turbulence values can give a reasonable look into a flow, and

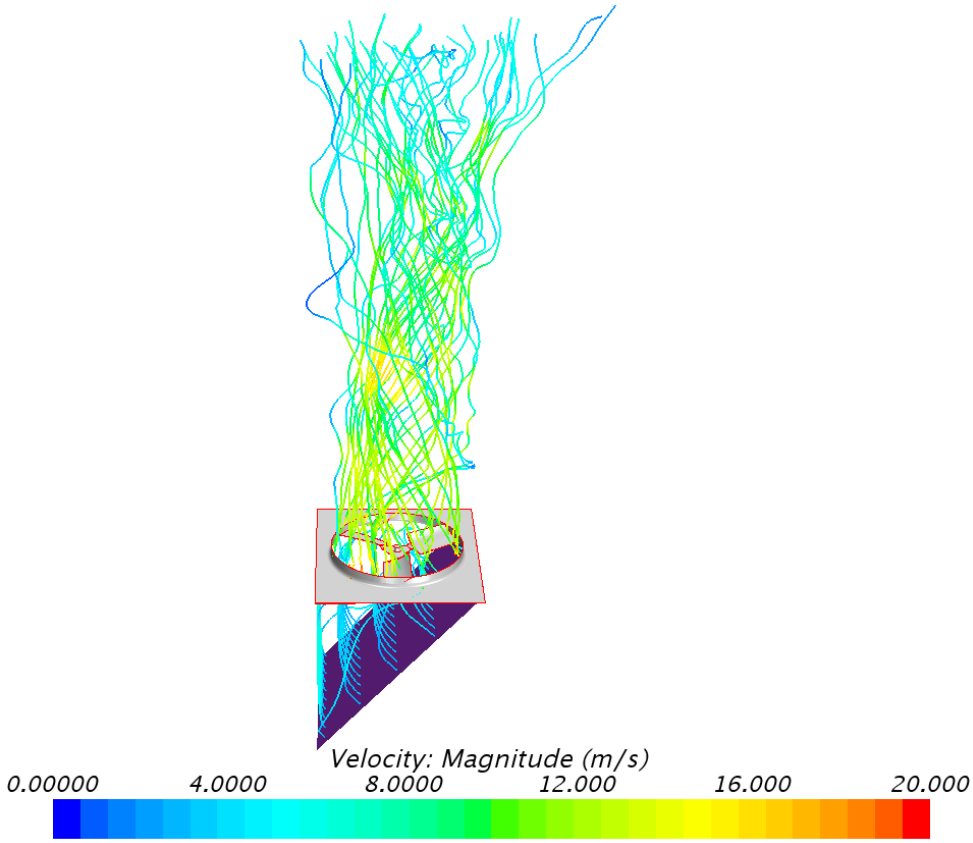

Figure 2.13: Streamlines tracing flow from inlet to outlet of the fluid domain, which help in identifying reversed flow, or turbulence and swirl locations

its areas of interest.

Velocity can provide a look into multiple aspects of the flow and flow structure. The raw values of velocity can be used to determine how a particular flow field is performing when compared to experimental or expected values. Or, velocity values can be compared against other simulations when studying the effects of different design changes.

The distribution of velocity values can also be a useful parameter. Flow distribution can greatly contribute to system efficiencies and vibrations such as in heat transfer across a coil, or rotor imbalance. The distribution is a look at how the

velocity values vary across a particular section of flow. The expected distribution of a certain flow can vary widely, and therefore, the particular application of the flow must be considered when determining if the distribution deviates largely from expected values. The distribution can then be used to implement design changes that contribute to a better distribution that would increase performance for the particular application.

Velocity can also be used at a particular location to determine if turbulence exists within the region. The average velocity at a discrete location can be compared to the deviation of the velocity values over time. Higher values of standard deviation of the velocity indicate that higher levels of turbulence are present.

Turbulence and turbulent flows are classified by a velocity field with chaotic fluctuations and structures. The amount of turbulence contained within a flow can be numerically investigated through various equations. The turbulent kinetic energy (TKE) is often used to characterize the amount of turbulence in a flow. TKE is the root-mean-square of the velocity fluctuations, which gives the kinetic energy per unit mass. Turbulence intensity (TI) is another value that can help characterize a flow. TI is the ratio between the fluctuating portion of velocity, and the average value of velocity. It gives a normalized look at how much the velocity is fluctuating at a point or across a region. Turbulence tends to dissipate as flow progresses without the addition of outside forces. This is due to the breakup of turbulent structures into continually smaller structures, until viscous shear stresses convert the kinetic energy to thermal energy. Numerically, this is represented by the turbulence dissipation rate, which is a shear stress calculated with a local turbulent viscosity and the average strain rate tensor. Turbulence often leads to rotations within the flow that can be seen as a vortex. Rotational flow is often called vorticity, and is numerically calculated as the curl of velocity, and is twice the rotation of the fluid at a point.

CFD is a valuable tool for analyzing and characterizing flow fields. Many other parameter values can be used in CFD to aid with investigating the flow field. A CFD user is expected to know how to modify a model and data collection tools to accurately analyze and understand specific fluid problems before a simulation is ran. in order to collect the correct data before a simulation is ran.

CFD Geometry Simplifications

The real-world geometry of research objects, is generally complex, and can be simplified in many ways to reduce design and computational time without drastically influencing the flow field effect. One simplification often made is reducing the complexity of the geometry by entirely eliminating certain features. In a flow with large scale turbulence, features such as manufacturing defects or hardware may only add small scale turbulence that is quickly dissipated. Therefore, including these features in the geometry would only add computational time with little effect on the bulk flow.

Other simplifications can be made to keep certain characteristics of a geometry that are important to the overall flow. Such a simplification can be done with a porous surface in order to keep the pressure drop characteristics of a surface which is dependent on velocity and inertial and viscous effects. Such porous media is governed by the Reduced Forchheimer's Equation given by,

$$-\Delta p = P_v v + P_i v^2 \tag{2.8}$$

where $-\Delta p$ is the pressure drop across a porous surface, P_v and P_i are the influence of viscous and inertial losses, respectively, and v is the local velocity on the porous surface.

The inertial and viscous coefficients are generally found experimentally, by

collecting velocity and pressure data on a surface. This data is then fit with a second order trend line, and the coefficients are extracted from the equation of the trendline.

Error and Limitations

CFD is continually advancing in its ability to aid in flow field investigation, however, errors and limitations do exist within the field [30]. There are inherent errors in CFD as the discretization approaches discussed earlier, are only approximations of the governing equations, resulting from discretization error. Another source of error comes from round off error, resulting in computers rounding error to a certain number of significant figures. Double-precision machines are commonly used today, which round to 15 significant figures. With such precision, round off error is often insignificant when compared to discretization error. The human interaction with CFD can be a large source of error within any model. Such error can exist due to users misrepresenting geometry within a problem by improper or coarse meshing or incorrect CAD. Other human error arises from misusing physical models chosen, such as choosing inappropriate turbulence models.

One of the largest limitations of CFD is computational expense. High performance computing has allowed for larger models, both in simulation time, or simulation domain, to take place. However, modeling increasingly complex problems are often limited by this computational time. This limitation is most often dealt with by reducing the complexity of a particular problem to only look at a broader view of the flow physics. Other limitations include the uncertainty contained within computational models, such as representing turbulence numerically. Uncertainty across CFD as a whole, leads to the need to verify computational models with physical models. Despite the errors and limitations of CFD, it remains a significant and useful tool across many fields of engineering.

Data Analysis

Analyzing the results from a multi-variable input to determine relationships, trends, and provide a direction for optimization, can be done in a number of ways. This research used a Response Surface Methodology (RSM) to optimize the inlet and outlet curvature sections. RSM is a set of techniques to both understand the effect of different paramaters or variables on a certain outcome of interest, and then determine the optimal settings of those variables to produce the best outcome [38]. In RSM, 'factors' are input variables that can be controlled in a given experiment. When a factor is changed, it is expected to have an effect on the response variable, which is a measured quantity that is influenced by the factors.

The true response is assumed to be a continuous function which depends on any number of factors given by,

$$\zeta = \phi(X_1, X_2, ...X_k) \tag{2.9}$$

where ζ is a vector of responses, ϕ is the true response function, and X is a vector of factor values up to some number of factors, k. This function can be represented locally at an arbitrary point using a Taylor-Series expansion. Using just one factor, this expansion around an arbitrary point a is given by,

$$\zeta = \phi(a) + (X_1 - a)\phi'(a) + 1\frac{1}{2}(X_1 - a)^2\phi''(a) + ... \tag{2.10}$$

where ϕ' and ϕ'' are the first and second derivatives of the true response function with respect to the single factor X_1, evaluated at a. The series expansion can be reduced to,

$$\zeta = \phi(X_1) = \beta_0 + \beta_1 X_1 + \beta_2 X_1^2 + ... \tag{2.11}$$

where β are coefficients which depend on a and the derivatives of $\phi(X_1)$ at a.

The resulting fit equation can be used to any number of degrees by increasing the number of terms kept in the Taylor series expansion. Using the one factor example, truncated at the second degree, giving,

$$\zeta = \beta_0 + \beta_1 X_1 + \beta_2 X_1^2. \tag{2.12}$$

This yields the equation for a parabola, whereas a first-order would see $\beta_2 X_1^2$ eliminated, and the result is a line fit.

RSM can be used with multiple factors at once, optimizing over a set of conditions. The second order fit for a multiple factor problem is given as,

$$\zeta = \beta_0 + \sum_{i=1}^{k} \beta_i X_i + \sum_{i=1, j \leq 1}^{k} \beta_{ij} X_i X_j \tag{2.13}$$

where i and j represent the number of responses up to k. This research looked at two factor problems with a single response, resulting in the following fitting equation giving a parabolic surface fit to the data

$$\zeta = \beta_0 + \beta_1 X_1 + \beta_2 X_2 + \beta_{11} X_1^2 + \beta_{12} X_1 X_2 + \beta_{22} X_2^2. \tag{2.14}$$

Equation 2.14 was used with known inputs for X_1 and X_2, and the measured response, ζ. The coefficients, β, were then solved for, optimization equation that could be used to find the maximum response, and the input variables to achieve that response.

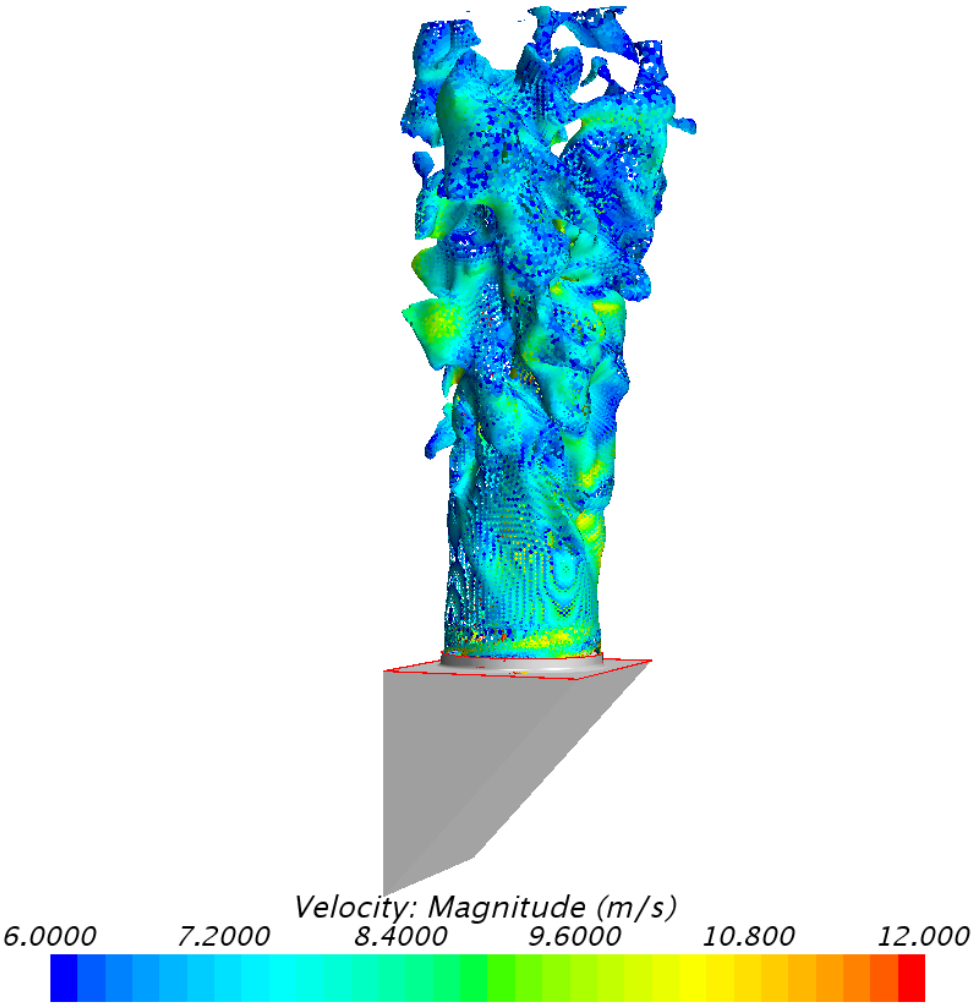

Figure 2.14: Isosurface of velocity ranging from 6-12m/s, which helps outline specific areas of flow based on the value of interest

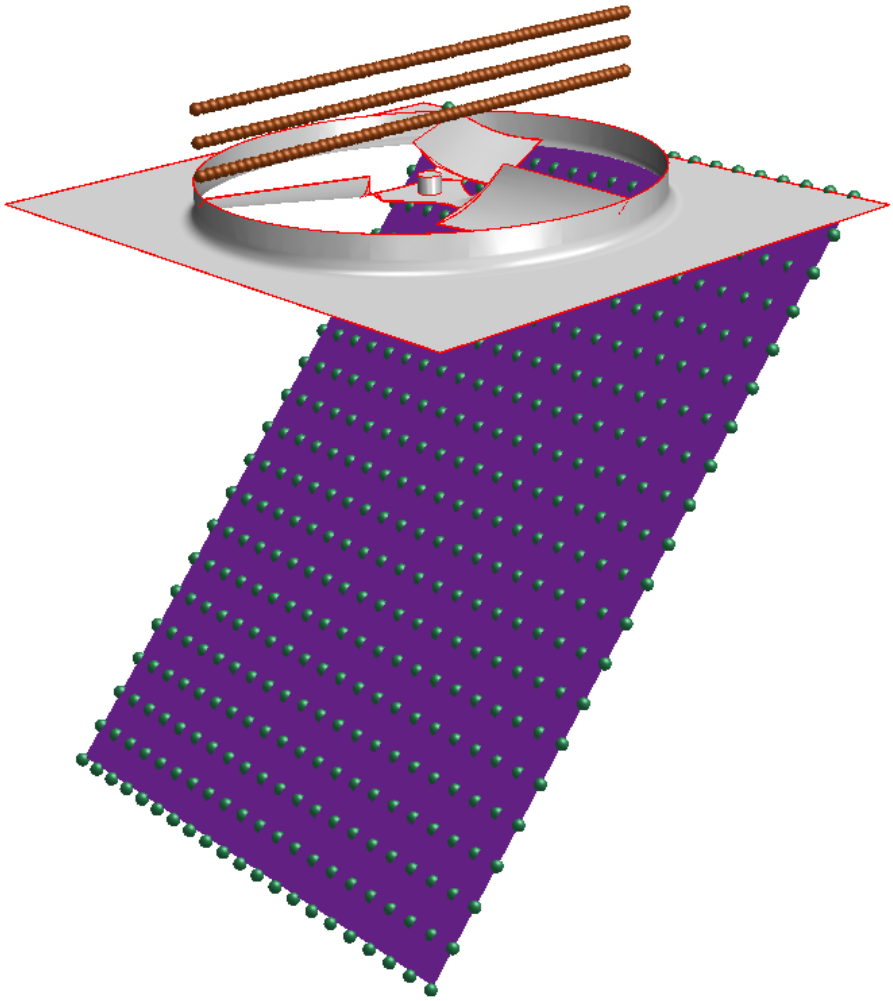

Figure 2.15: Line and grid probes placed within the fluid domain

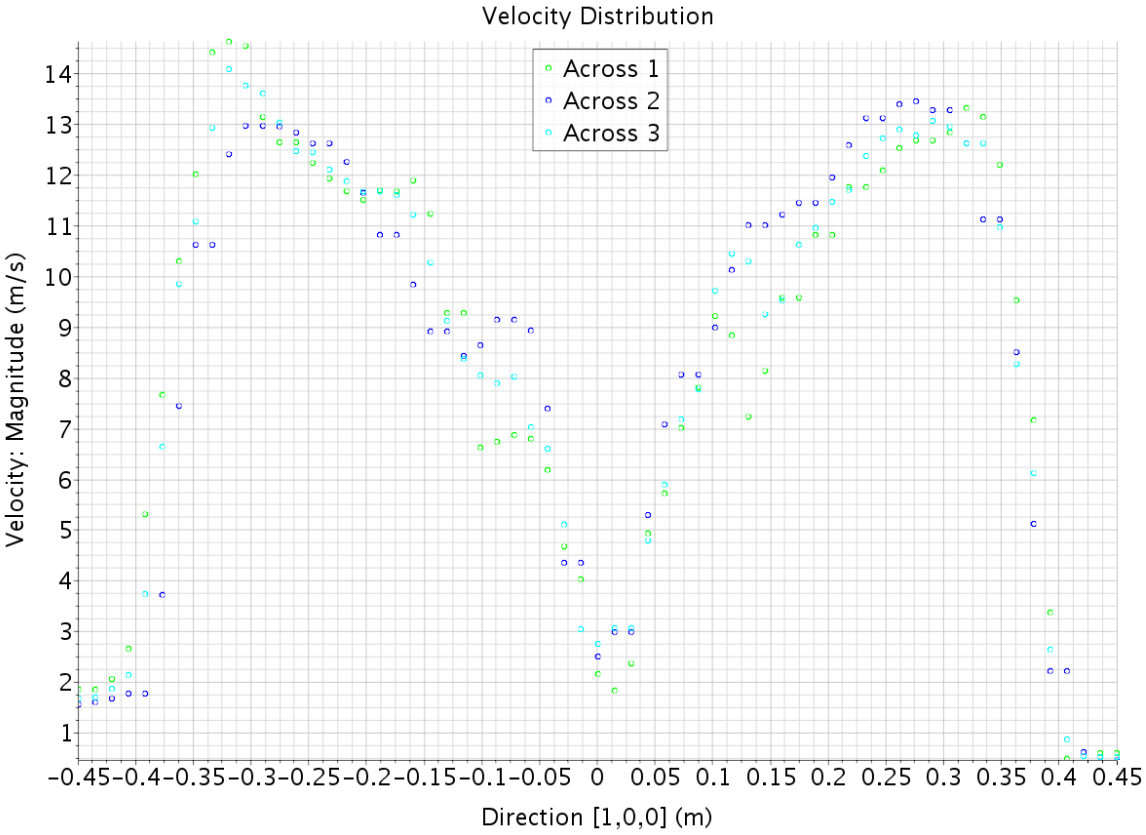

Figure 2.16: XY plot of velocity distribution downstream of a condenser unit fan

CHAPTER THREE

EXPERIMENTAL METHODOLOGY

The experiments conducted on the condenser unit for this research were performed to help model the condenser coil in the CFD simulations and to validate the results of the simulations. The experimental object in these experiments was a condenser unit which produces flow using a 3-blade aluminum axial fan run by a 560W motor rotating at 1100 revolutions per minute (RPM). The equipment used to measure experimental data included a TSI 9535 air velocity meter (± 3% error) to measure air velocity, an Alnor AXD 560 micromanometer (± 1% error) with static pressure probe to obtain pressure data, and a Monarch Nova Strobe DB Plus 115 stroboscope (± 0.001% error) to measure the rotational speed of the fan in RPM. The unit and experimental setup can be seen in Figure 3.5.

Porosity Data

The coil geometry is complex (Figure 2.3), and would be difficult to represent sufficiently detailed for a fluid model. Furthermore, if the geometry was recreated properly, the resulting mesh fineness needed would result in a highly computationally expensive model.Therefore, the condenser coil is modeled as a porous region in the CFD simulations. This saves computational expense by avoiding a highly complex geometry in the simulation leading to increased mesh cell count. To model a porous region, a user input of resistance values is required to accurately model the pressure drop that exists across the region. These inputs are derived experimentally by collecting a pressure drop across the physical surface over a range of velocity values. These experimental pressures and velocities are then used in the Reduced

Forchheimer's Equation given by Equation 2.8.

Five different measurements were taken from the coil, and an assumed zero pascal condition was set for a zero velocity condition. Since the coil was exposed to atmospheric conditions, the pressure upstream is assumed to be zero pascals. A pressure probe was used to measure the pressure directly downstream of the coil surface. At the same location, the air velocity meter was used to measure the air velocity. The results were graphed, and a 2nd-order polynomial was used to fit the data to model the Reduced Forchheimer's Equation (Figure 3.1). The coefficients of the data fit were used as the resistance input values required to model the coil as a porous region. The constants given by the trend line are then used as the viscous and inertial coefficients, giving $P_v = 17.246$ and $P_i = 1.9252$ for the coil.

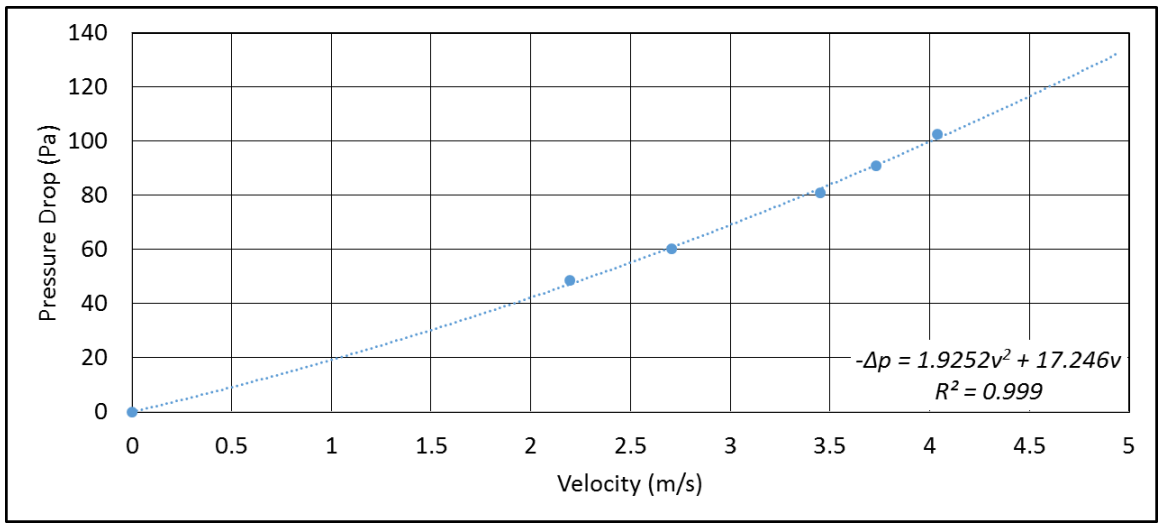

Figure 3.1: Experimental pressure drop and velocity data with quadratic fit

Velocity Data

To use CFD as a design iteration tool, the simulation results must first be validated to ensure that the correct physics are being modeled, and that any

simplifications made to reduce computational expense are not largely altering the flow dynamics. To validate the CFD results, a series of velocity measurements were taken above the fan. The locations of the physical data were recorded, and line probes were placed in the CFD simulation at the same location in order to compare the results. The air velocity meter sensing probe at the tip is partially shielded as shown in Figure 3.2. This resulted in the velocity measurements consisting of mostly z-component of velocity with slight influences from both x and y components of velocity.



Figure 3.2: Partially shielded TSI 9535 air velocity meter probe

To validate the CFD results three horizontal traverses were done to collect velocities at the front, side and back of the unit in the outlet region above the fan. Each traverse consisted of eighteen measurements from the center of the fan to 0.457m outward, seen in Figure 3.3 and three vertical collection points, each 0.05m apart (Figure 3.4). A test stand was used to hold the air velocity meter to ensure a straight line traverse. The Stroboscope was used to measure the rotational speed

of the fan in RPM. The motor was rated to operate at 1100RPM, and flash rates recorded, indicated the rotational speed did not deviate more than ± 0.73%.

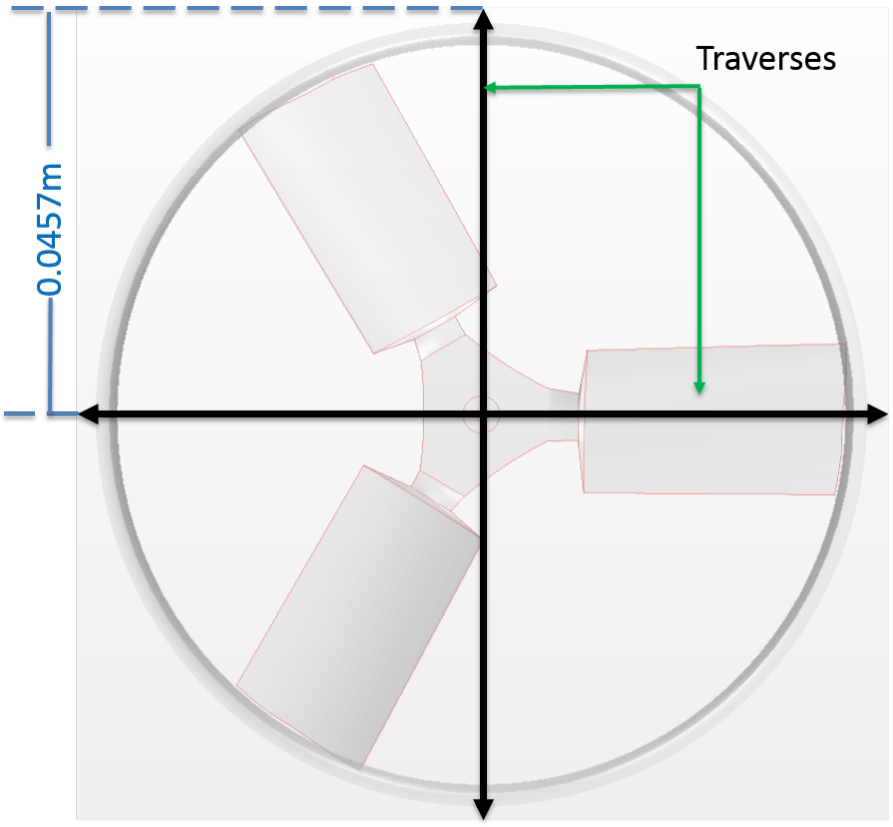

Figure 3.3: Three vertically placed horizontal velocity traverses



Figure 3.4: Three vertically placed horizontal velocity traverses

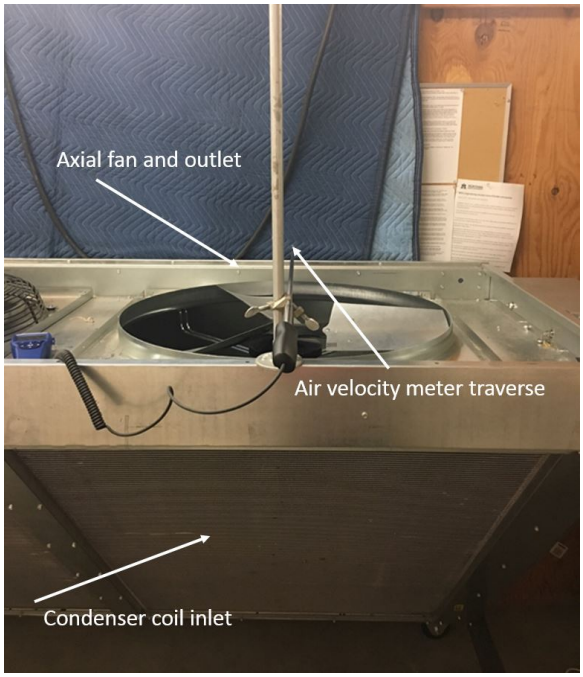

Figure 3.5: Experimental setup for condenser unit

CHAPTER FOUR

COMPUTATIONAL FLUID DYNAMICS METHODOLOGY

CFD has become an invaluable tool in the design process. It can be used to quickly change and evaluate the effects of design changes, allowing designers, to iterate and converge on final designs faster. This project aimed to use CFD in the design process of an orifice plate surrounding an axial fan, utilized by a condenser unit. A CFD commercial package, Star-CCM+®, was used to model, visualize and analyze the flow. This section summarizes the methods used to model the condenser unit, and the subsequent flow analysis.

Model Simplifications

Geometry

For this project, the 3D modeling tools within Star-CCM+® were used to create the geometries of the condenser unit. Small geometry features, such as bolts, screws and manufacturing defects were ignored due to the insignificant effects they have on the flow. The fan created is a 3 bladed, 25° pitch, 0.758m diameter fan. The coil inlet has a height of 1.346m and width of 0.940m. The unit top measures 0.991m from the front to back, and 1.118m across. The final 3D model used in the CFD simulations is shown in Figure 4.1.

Inlet

The fluid domain of interest to this project is located inside the condenser unit and in the region above the fan discharge area. Additionally, the condenser coil can be assumed to act as a flow straightener, causing the flow downstream of the coil to enter normal to the inlet. Because of these assumptions, the inlet to the computational

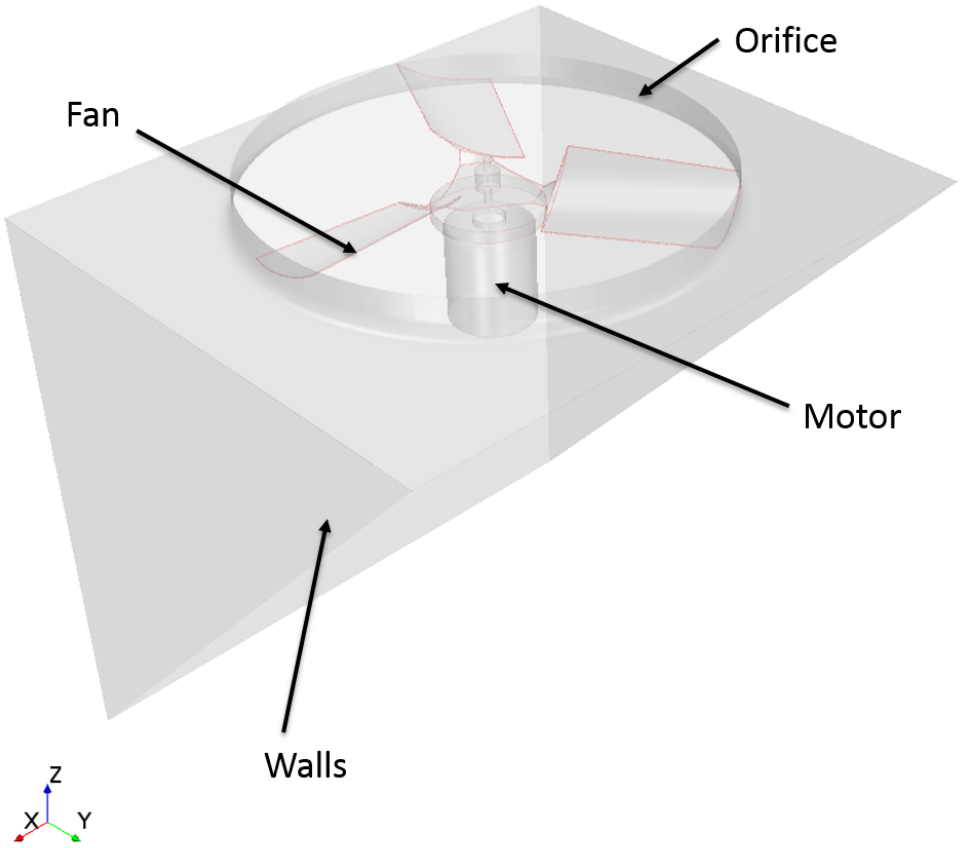

Figure 4.1: Simplified geometry of condenser unit

domain was chosen to be directly at the coil. To provide a more time-efficient model for this research, the coil was represented as simple rectangular region that could produce a pressure drop. This would provide a less accurate fluid domain near the coil, as small scale turbulence and mixing effects would not be represented. However, since such effects were not the main interest of this research, and the coil was only necessary to control mass flow rate through the fluid domain, such representation of the coil is acceptable.

A porous inlet condition is available in Star-CCM+®, where P_v and P_i are user-defined inputs. P_v and P_i are inherent to a given porous media, and are generally found experimentally. The porous inertial and viscous coefficients for the coil in this

research were found experimentally, and are $P_v = 17.246$ and $P_i = 1.9252$.

Outlet

The outlet for the experimental data was to atmospheric conditions giving an outlet pressure of 0.0 Pa. Star-CCM+® applies an outlet condition where the pressure must be defined. To match experimental work, the pressure was set to a constant 0.0 Pa. With these conditions set in the simulation, the outlet domain requires sufficiently large space to meet the outlet pressure condition. Reducing the outlet domain can force unrealistic back flow at the condenser unit outlet in order satisfy the pressure condition. Therefore, the outlet domain was increased until back flow was sufficiently reduced.

Model Parameters

Star-CCM+® requires a physics continuum to be specified for a simulation. This requires the user to specify models necessary to represent and solve the given flow field. For this project, an ideal gas model was used for the properties of air, allowing for density changes based on pressure. The flow was specified as turbulent, as the Re is well above a laminar range. A DES was used to capture turbulence effects without increasing computational costs that arise from LES simulations. The reference pressure was set to 84,940Pa which corresponds to atmospheric pressure at 1463m; the elevation where the experimental data was collected. An unsteady simulation was ran since the turbulence structures and flow field are varying.

Simulation

A moving reference frame was used to rotate the fan at 1100RPM, which corresponds to the operating speed of the experimental fan. The time step was set to

Table 4.1: Physics parameters for CFD simulation

Fluid model	Ideal Gas
Working Fluid	Air
Flow Type	Turbulent
Turbulent Solver	DES
Reference Pressure	84,940Pa
Simulation Type	Unsteady

1.5152E-4s which allows the fan to rotate 1° with every time step. Within each time step, 7 inner iterations are used to reach convergence of the time step. Lastly, the total simulated time was 1.5s which allows the fan to rotate 27.5 times, and reaches good convergence of the parameters of interest.

Table 4.2: Simulation parameters for CFD model

Rotation rate	1100RPM
Time-step	1.5152E-4s
Inner Iterations	7
Run time	1.5s

Data Collection

For this project, a variety of parameters were of interest, including velocities, pressures, mass flow rate, moment, TKE, and vorticity.

Velocity was collected in both a vector scene, and from line probe data traversing the inlet and outlet of the fan, and a grid probe at the coil inlet as shown in Figure 4.2. The line probes span from the front to back of the fan and across, to see if

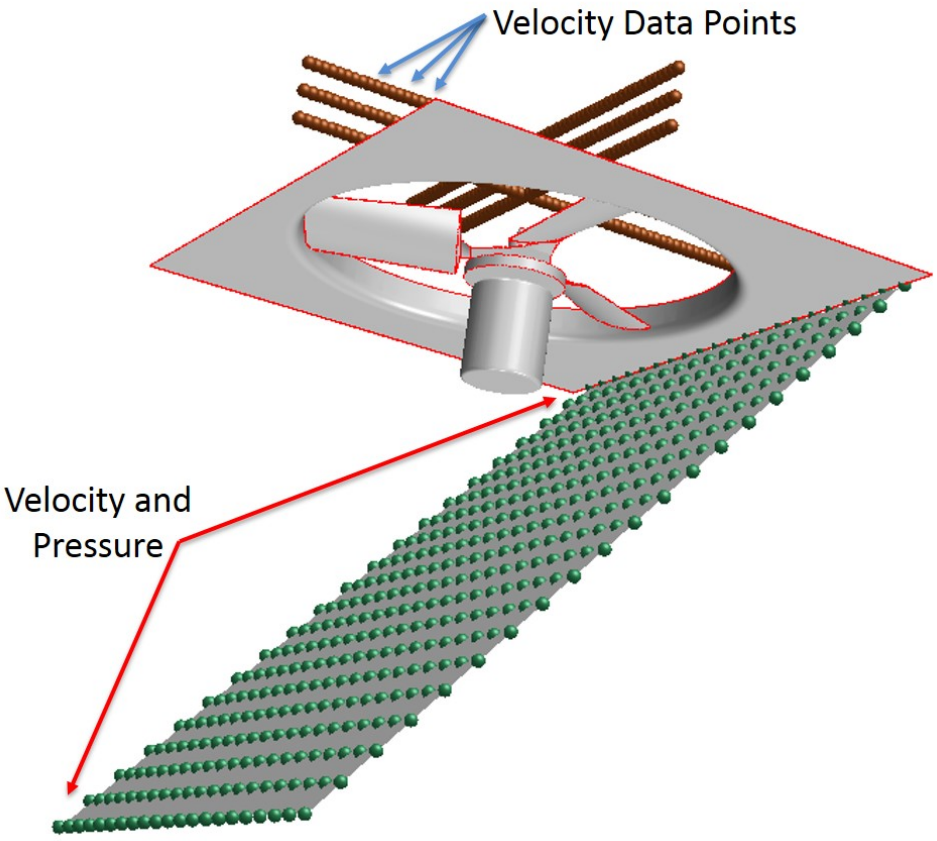

Figure 4.2: Line probe and grid used for simulation data collection

there are varying effects in different azimuthal locations. The probes were also placed at different z-locations to study the velocity profile as it progresses further from the fan. The grid at the inlet was used to see the flow distribution across the coil both vertically and horizontally.

To assess the performance of the fan using the fan efficiency equation (Equation 2.7), a pressure drop was recorded by collecting the pressure from the inlet surface and assuming the outlet surface was zero pascals. Mass flow rate was collected at both the inlet and the outlet, and helped ensure conservation was met through the

simulation. The mass flow was also converted to a volumetric flow rate using,

$$VFR = \frac{\dot{m}}{\rho} \tag{4.1}$$

where VFR is the volumetric flow rate, $\dot{m}$ is the mass flow rate, and ρ is the density. Lastly, the moment around the z-axis was collected on the fan and converted to power using,

$$W = M\omega \tag{4.2}$$

where W is power, M is the moment, and ω is the angular velocity of the fan in $\frac{rad}{s}$.

TKE and vorticity can affect the performance of the fan and condenser unit. These parameters were studied in scaler scenes and with isosurfaces to see the effect of turbulence and rotational effects imparted on the flow upstream and downstream of the fan.

Model Validation

The locations of the line probes placed within the CFD simulation were chosen based on the physical experiments. Having the line probes in the same location, allows for the velocities at those locations to be compared to experimental results. The data collection device used for velocity readings cannot collect on the same timescale as the time step used in the simulation. Therefore, the CFD data was collected at every time step, and was then time-averaged to compare to the experimental values. Both the magnitude and general trends of the velocity data were analyzed to ensure the simulation was capturing the physics of the real-world unit.

Redesign

The redesign aimed to increase the effectiveness of the coil and fan, and reduce noise emitted from the unit. The fan-orifice interaction can be redesigned in a number of ways, including changing the location of the fan, the length of the outlet, or by serrating the outlet surface of the orifice plate [19]. This project aimed to quantify the effectiveness by changing both the inlet region and outlet region of the orifice plate independently, and specifically how the curvature in these regions affects the flow.

To analyze the performance of the redesigned geometries, a number of parameters and values were studied. Because the bulk volumetric flow rate translates to a faster flow velocity, which improves heat transfer at the coil face, the mass flow rate and density were collected. The pressure at the inlet was collected at the coil face to find the pressure drop across the fan, for use in the fan efficiency equation. The moment on the blades was collected to use in Equation 4.2 to calculate power into the fan. TKE, velocity and pressure were also used to both qualitatively and quantitatively examine turbulent regions in the flow.

Current Orifice

The current orifice geometry is a simple stamped aluminum piece. The geometry, shown in Figure 4.3 and 4.4, has a curved region with a width of 0.027m and a height of 0.025m. The orifice extends with a straight vertical section for 0.038m, and the fan is placed within the orifice plate with the top of the blades flush with the top of the orifice.

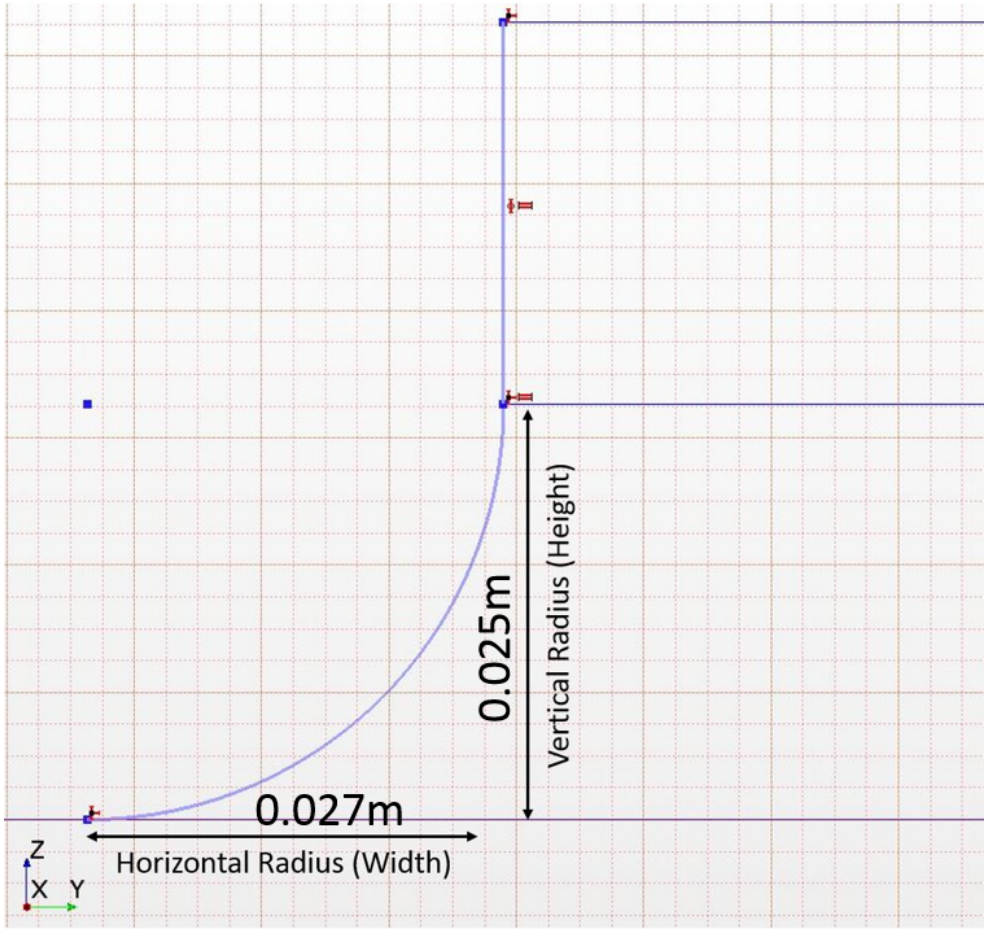

Figure 4.3: Current geometry sketch

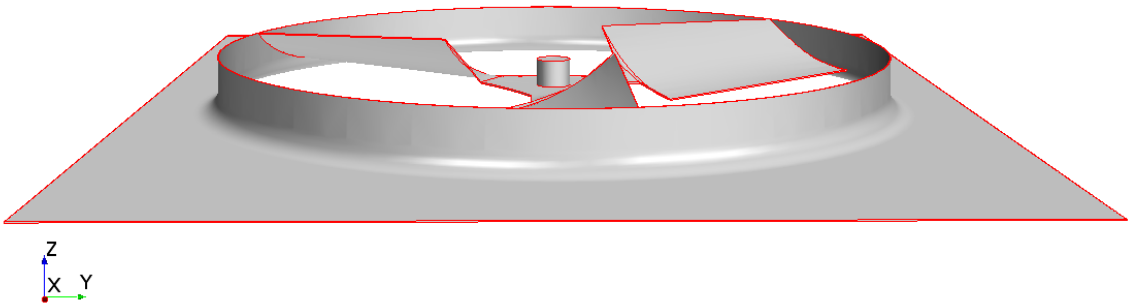

Figure 4.4: Current geometry with fan placement

Orifice Inlet

The inlet region of the orifice plate is just upstream of the fan and directs flow into the fan. In order to understand the effects the inlet curvature geometry might have on the fan performance, 18 redesigned geometries were simulated. The geometry of this region was changed using a quarter-ellipse with changing width and height. An example geometry with a 0.045m width and 0.065m height is shown in Figure 4.5. The straight section of 0.038m was kept constant for all changing inlet geometries, and the top of the fan blades were kept flush with the top of the orifice as shown in Figure 4.6. The simulations were run with varying inlet width up to 0.045m which was the maximum width before the inlet would be too large to fit on the unit, and the height was run through 0.085m as larger heights would be impractical from materials and shipping costs.

First, the inlet geometry was changed by widening the inlet with 5 different constant curvature cases, where the inlet width is equal to inlet height. Second, the effect of the height of the orifice was studied by vertically lengthening the orifices' elliptical shape while maintaining a constant inlet width. After the trends were studied independently, the effects of both inlet width and height effects were studied together using an RSM fit. The RSM fit was used to find a maximum response for both VFR and fan efficiency. The width and height found from the RSM to produce these maximum responses were then simulated.

A post-processing code was also developed to view and analyze the face velocity distribution on the coil surface. This was used to determine if the orifice could affect the distribution to improve overall efficiency of the condenser unit.

Additionally, a number of parameters were studied in scaler scenes and isosurfaces to understand the flow dynamics of the condenser unit, and how the flow changed from one design to the next. These values included TKE and pressure and

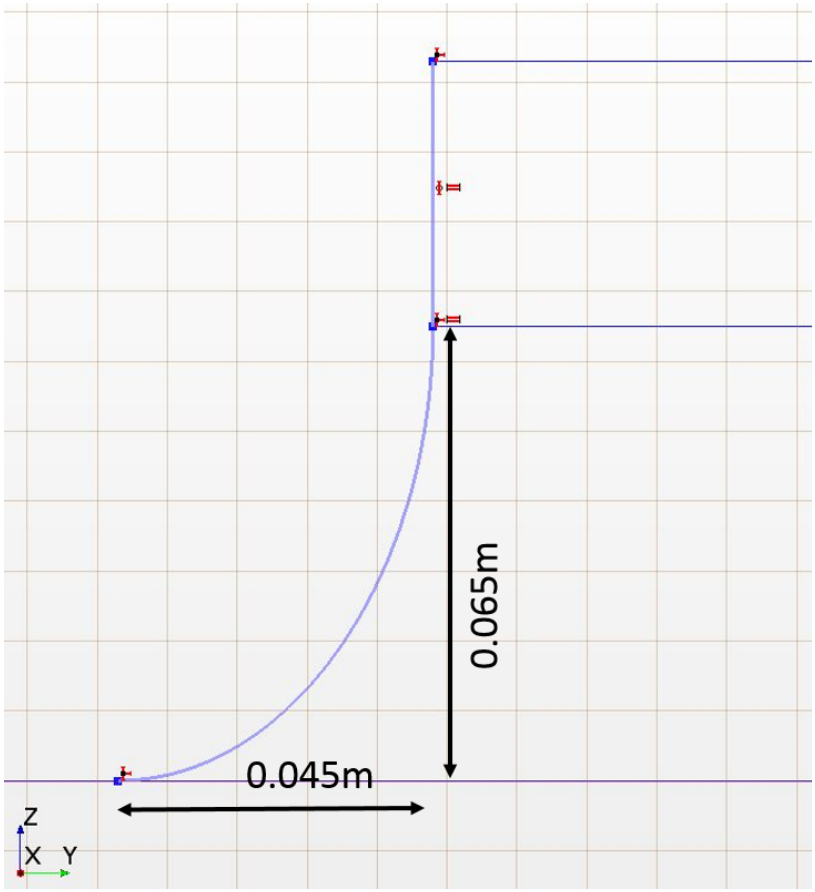

Figure 4.5: Example inlet geometry sketch

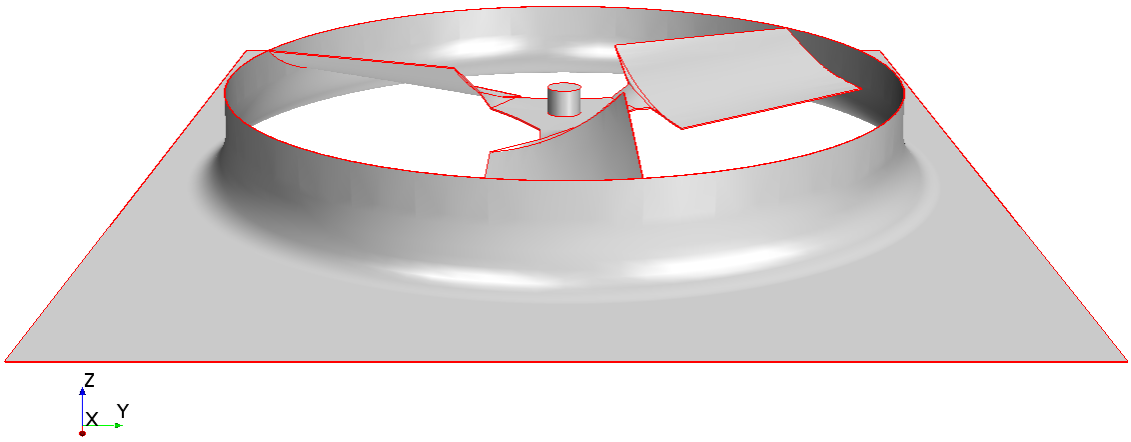

Figure 4.6: Example inlet geometry with fan placement

helped to understand how changes in VFR and fan efficiency developed, and what parameters most influenced them.

Orifice Outlet

The outlet region of the orifice plate is downstream of the fan and transitions the flow into the zero-pressure atmospheric condition. The geometry of this region was also changed using a quarter-ellipse with changing width and height. A total of 51 simulations were run, varying the width from 0.0m to 0.065m and the height from 0.0m to 0.130m. The original inlet orifice was used with the tops of the fan blades oriented flush with the top of the original geometry as the new outlet geometry was changed. An example geometry with a 0.035m width and 0.065m height is shown in Figure 4.7 and 4.8.

Post-processing codes were developed to look at correlation of the curvature on fan efficiency, and to create a 3D surface to show the trends with changing width and height at the outlet Again, a number of parameters were studied in scaler scenes understand the flow dynamics at the outlet region of the condenser unit, and how the flow changed from one design to the next. These values included, vorticity and pressure.

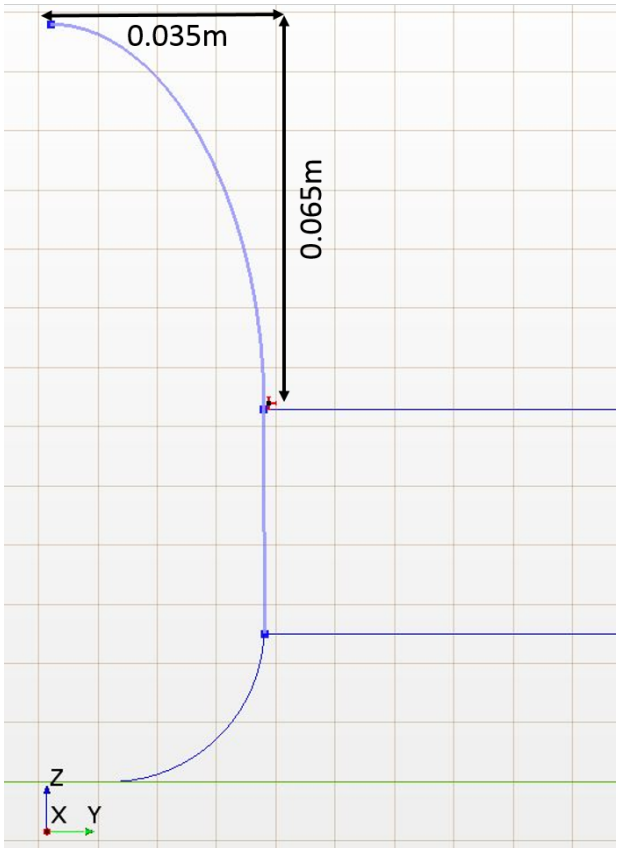

Figure 4.7: Example outlet geometry sketch

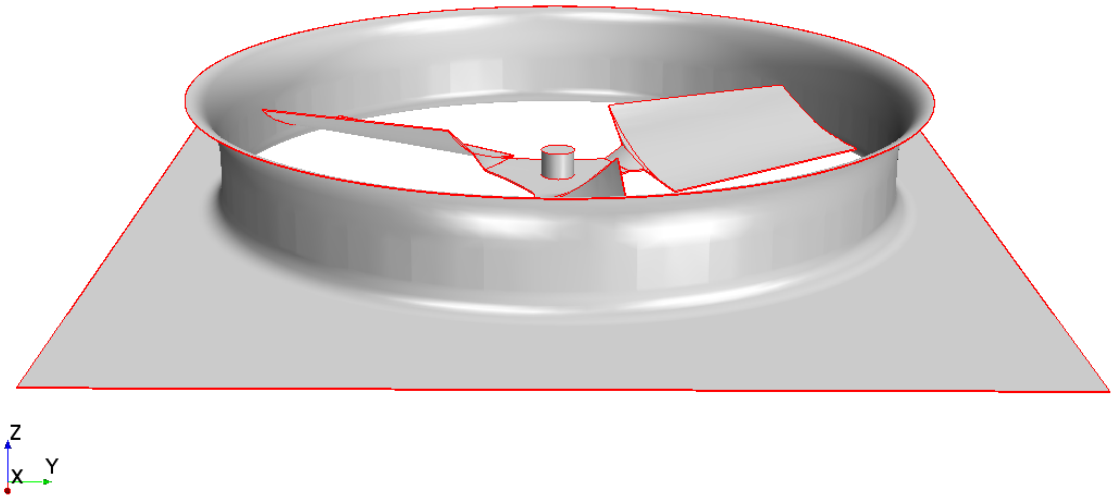

Figure 4.8: Example outlet geometry with fan placement

CHAPTER FIVE

RESULTS

The results from the experimental data, and the CFD simulations were used to analyze the flow characteristics of the condenser unit, and its performance. The CFD model was first validated using the experimental results for velocities at a variety of azimuthal locations around, and z-directions, above the fan. After reaching good agreement with the experimental data, showing the CFD model was performing well, the geometry of the orifice was changed in a number of ways. The mass flow, pressure difference across the fan, and power of the fan were all used to analyze the performance of the fan. Velocities on the inlet were used to visualize the distribution of the flow at the coil surface, and the vorticity and TKE were used to analyze the turbulence in the system. After converging on a redesigned geometry with optimal performance for both the inlet and outlet regions independently, an orifice with the combined geometries was simulated.

CFD Validation

The velocity readings taken from the experiment were used to validate the CFD model. In the CFD simulation, the velocity was collected on the line probes at every time step. In order to compare this data to the experimental values, the CFD data was time averaged over the last ten revolutions of the fan. The standard deviation of the time averaged data was recorded, and the mean data was plotted with an error bar representing one standard deviation above and below the mean value. These error bars show areas where more turbulence exists, due to the increased fluctuation from the mean value. This can be seen with the increased error bar lengths near the middle of

the fan, and at the tip region. The magnitude and individual components of velocity were collected in the simulation. The z-component represents the velocity exiting vertically out of the unit, and is plotted for all velocity profiles. The experimental data is plotted with error bars representing the instrument error of the air velocity meter.

There is good agreement between the experimental and simulation data. The velocity profile at the back of the unit 0.0762m above the fan is shown in Figure 5.1. The magnitude of the simulation data over predicts and does not hold a similar trend to the experimental results until 0.15m from the fan center. In the region from 0m to 0.015m there is a velocity deficit due to the blockage upstream from the motor, which can be seen in the vector scene of velocity in Figure 5.2. This creates a highly turbulent region, and this trend is not captured by the air velocity meter probe due to its shielding around the collection point as shown in Figure 3.2. This shielding reduces, but does not eliminate, the influence of x and y components of velocity on the probe. Thus, the velocity recorded by the air velocity meter is assumed to be the z-component of velocity. Comparing the simulation values of z-component velocity to the experimental data, the two trends shows close agreement. The values of the experimental data are slightly above the simulation data due to the probes' minor influences from the x and y component velocities that are not present in the simulations' z-component data.

The velocity traverses on the side and front of the unit 0.0762m above the fan both showed good agreement to the z-component simulation data as shown in Figures 5.3 and 5.4. The front traverse has a slightly larger difference between the simulation and experimental data, due to the coil interaction at the front of the unit, causing higher turbulence not captured by the air velocity meter due to its shielding.

The additional traverses at vertical heights of 0.127m and 0.179m showed good

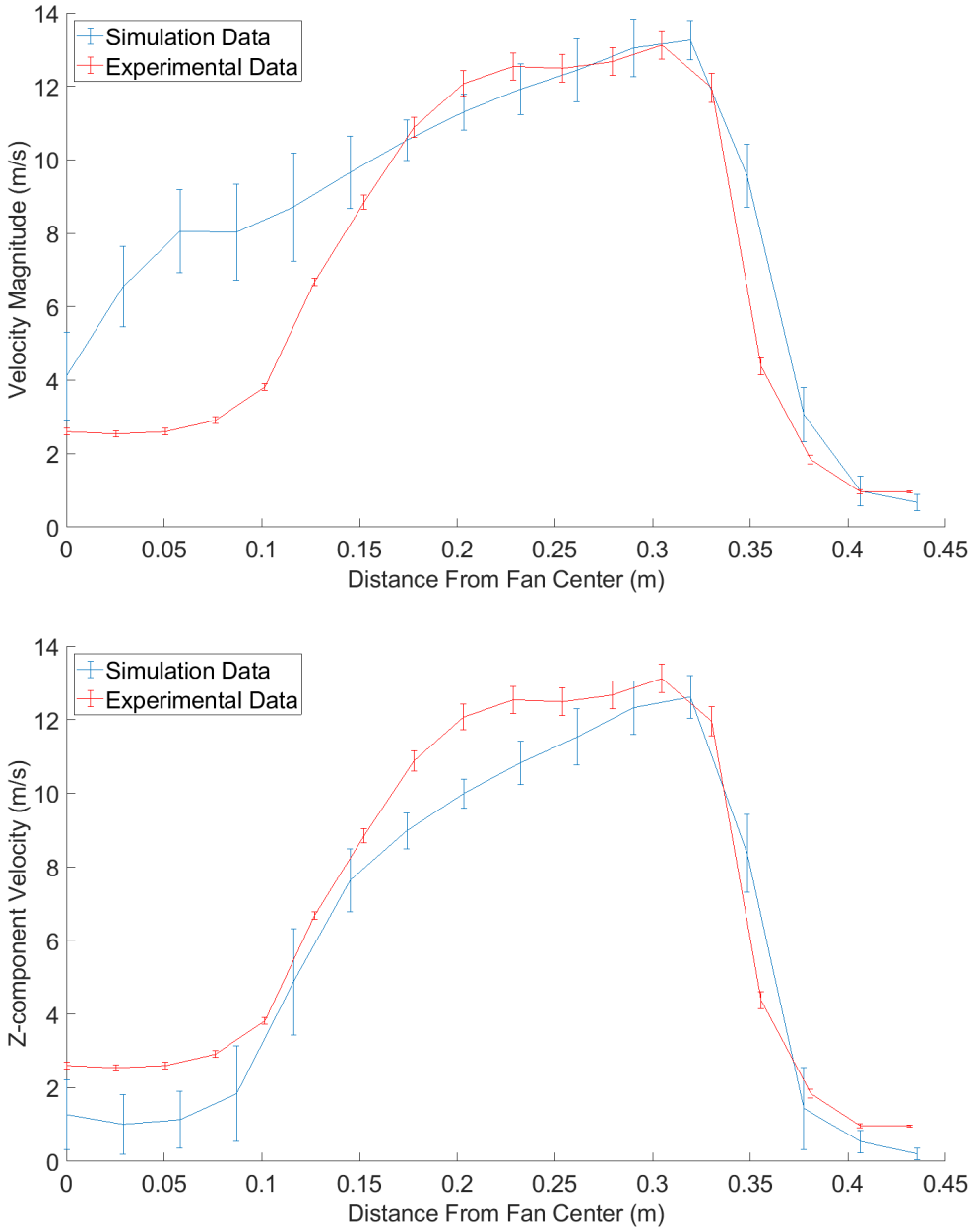

Figure 5.1: Velocity profile for center-to-back traverse magnitude (top) and z-component (bottom)

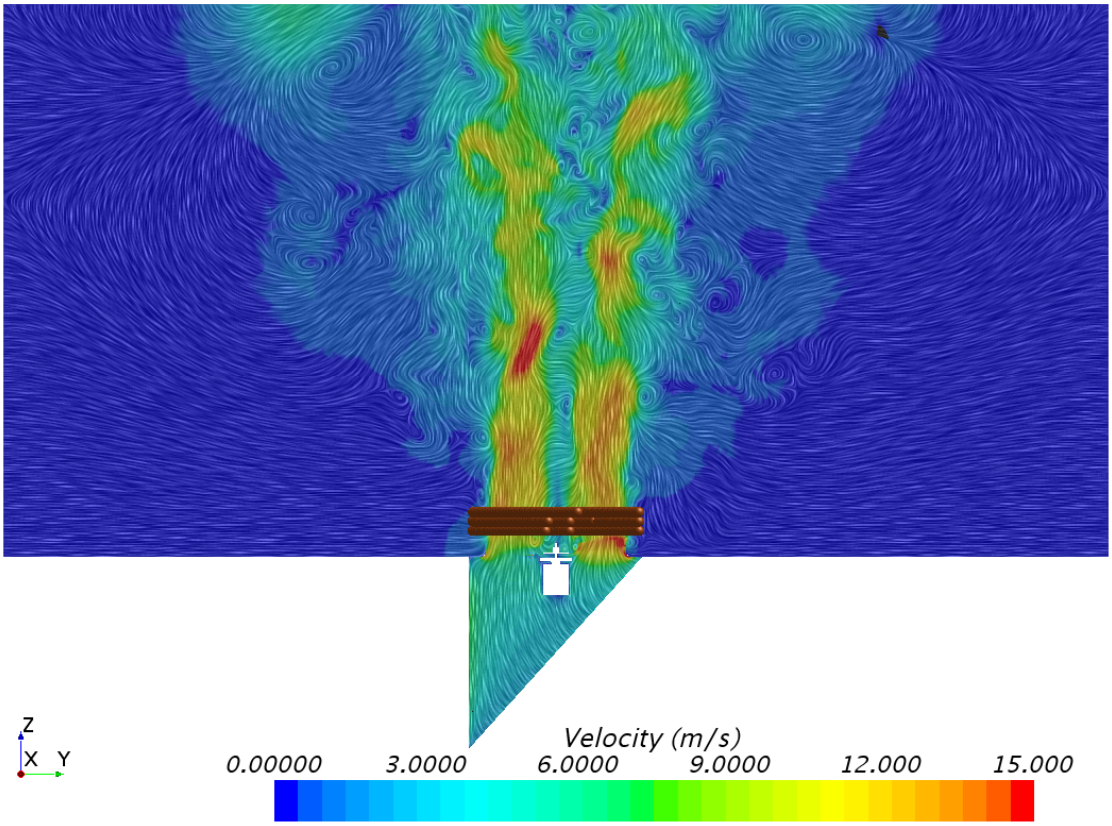

Figure 5.2: Velocity vector scene with velocity deficit due to motor.

agreement between experimental and simulation data (Figures 5.5-5.7). The velocity begins to decrease as the height away from the fan increases due to the dissipation of the high speed flow leaving the fan.

With the simulation velocity profiles closely following the trends and values of the experimental data, the CFD model is validated and can be used for redesign purposes.

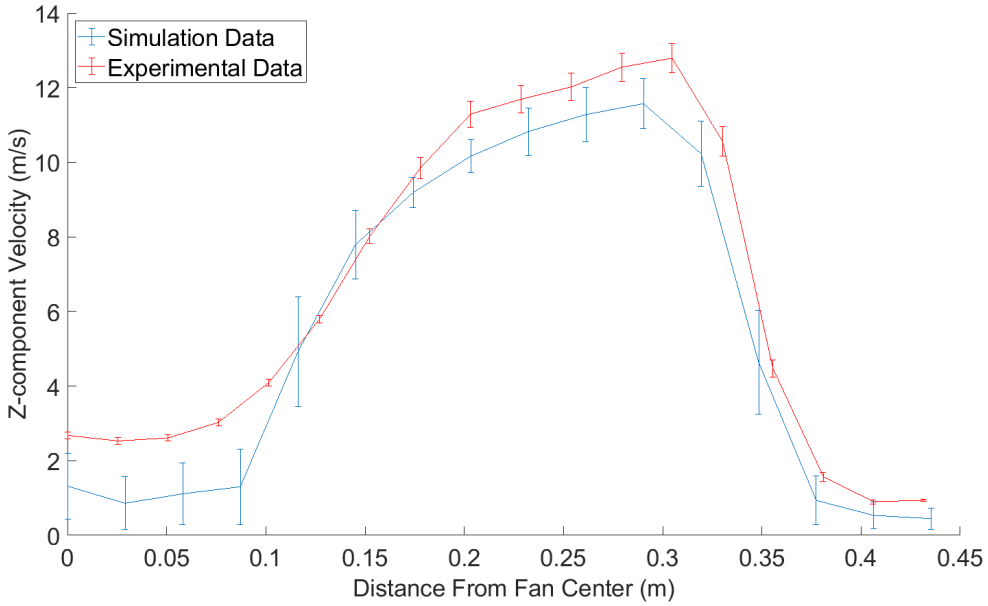

Figure 5.3: Z-component velocity profile for center-to-side traverse

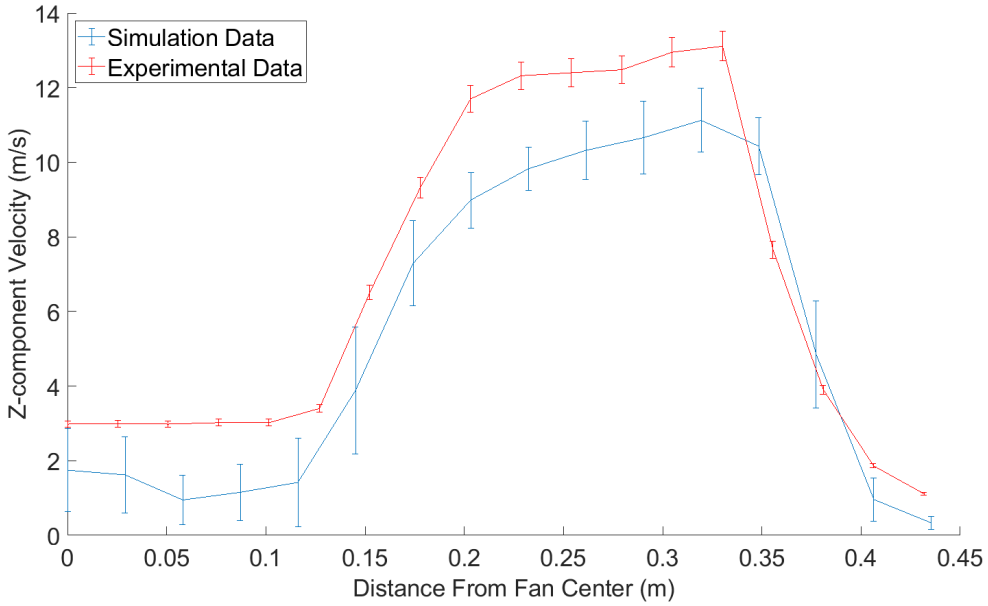

Figure 5.4: Z-component velocity profile for center-to-front traverse

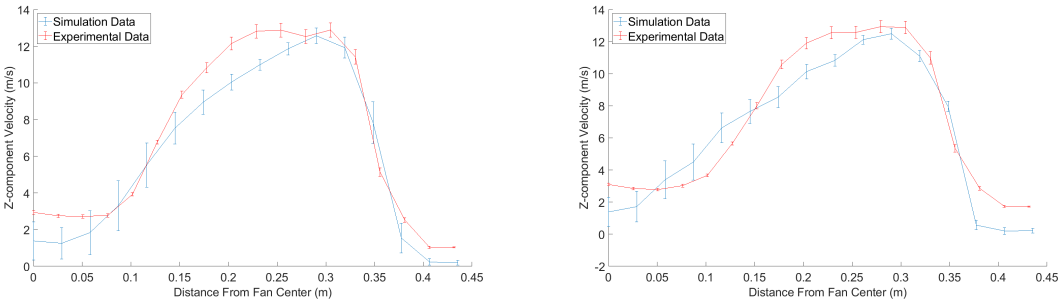

Figure 5.5: Z-component velocity profile for center-to-back traverse at vertical height of 0.127m (left) and 0.179m (right)

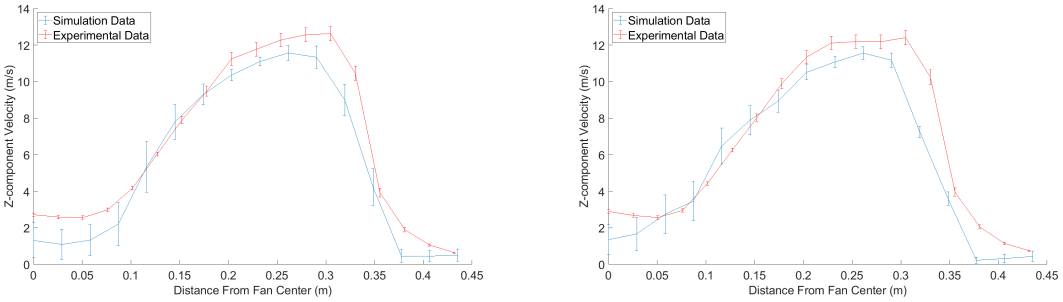

Figure 5.6: Z-component velocity profile for center-to-side traverse at vertical height of 0.127m (left) and 0.179m (right)

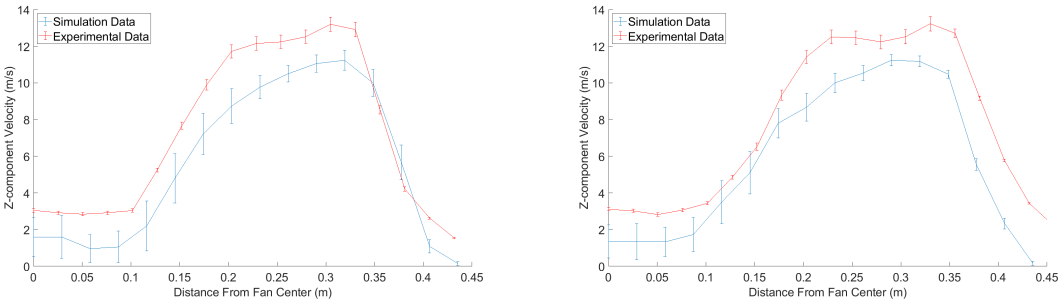

Figure 5.7: Z-component velocity profile for center-to-front traverse at vertical height of 0.127m (left) and 0.179m (right)

Redesign Analysis

In this section, the responses from the simulations for the orifice geometry changes are presented. The inlet curvature is first studied to show the effects on VFR, fan efficiency and inflow distortions. The outlet curvatures' effect on VFR, fan efficiency and outflow pressure fields are then presented. Additionally, the two regions were combined and analyzed to see if additional efficiencies occurred.

Inlet Curvature

The outputs from the 18 inlet orifice simulations were used to understand overlying trends that could influence the final orifice geometry. Results from the five simulations with orifice width and height increasing simultaneously with the same radii are shown in Figure 5.8. These results show that as the inlet is widened, the

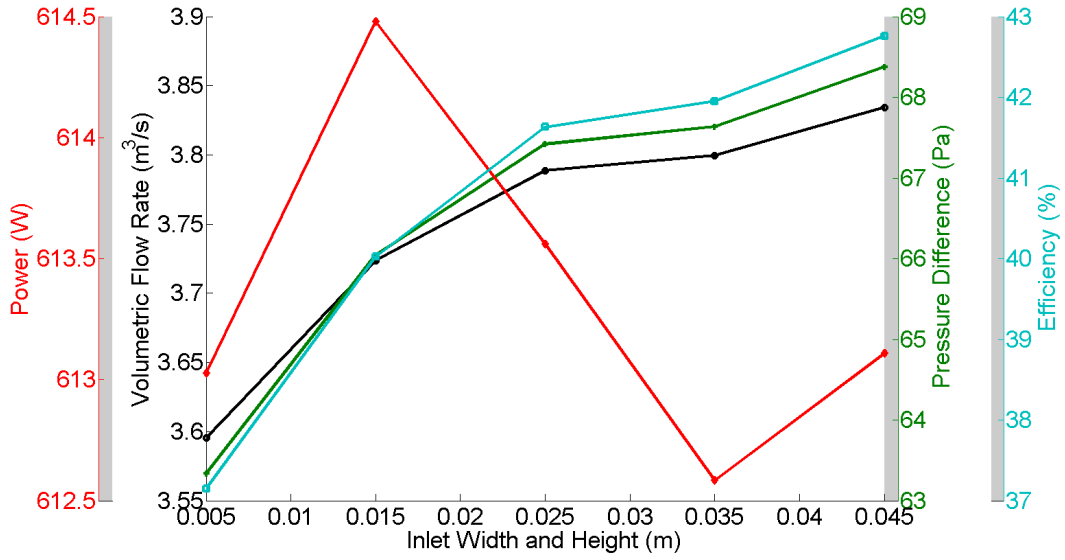

Figure 5.8: Constant curvature case with increasing width and height

VFR and pressure increase sharply at first, and then grow slowly until the largest radius is reached. The fan efficiency follows the trends of the VFR and pressure

closely, and has a fast increase for the first few curvature cases. The power required by the fan does not follow an obvious trend and the values only change a maximum of 0.25%. Since VFR, pressure and power all have a direct and equal influence on fan efficiency, power does not affect the overall fan efficiency as much as VFR and pressure which change as much as 3.59% and 3.93%, respectively. Though the trends begin to level, the highest VFR, pressure and fan efficiency were still found at the maximum allowable width and height.

The inlet velocity entering the fan region can be used to understand the trends seen with the increasing constant curvature. The velocity vector plot, shown in Figure 5.9, shows the direction of velocity, indicated by arrows, and the magnitude, indicated by color. The velocity direction enters the fan area in a more vertical direction, at the 0.045m constant curvature when compared to the 0.005m constant curvature at the same location and time step. The off-angle velocities with the 0.005m is due to the faster transition of the orifice from the horizontal velocities within the unit to the vertical flow direction through the fan and out of the unit. These inflow distortions and any flow separation into the fan, causes fan efficiency losses. To decrease these losses, smoother and longer transitions must be made to allow the flow to change direction, and enter the fan region more vertically.

Since the highest performance was found using the largest allowable width, a 0.045m width was used while changing the height between 0.005m and 0.085m. The results of increasing height are shown in Figure 5.10. The results show a similar trend to the increasing width. As the height increases with the fixed horizontal value, there is a quick increase in both VFR and pressure. The VFR and pressure begin to plateau toward the upper limit of the height before decreasing past 0.075m. Power again fluctuates, but does not influence the overall fan efficiency as much as VFR and pressure which change up to 3.01% and 3.60%, respectively, and power only changes

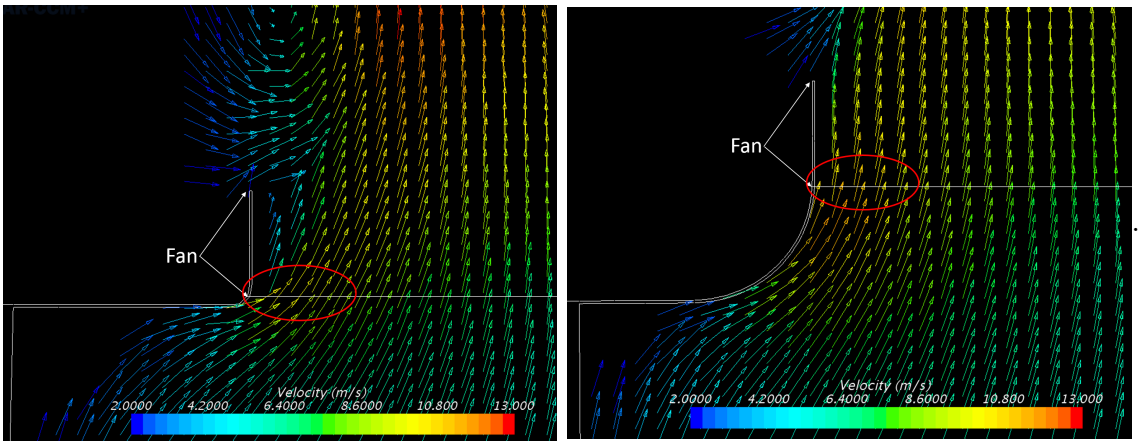

Figure 5.9: Velocity vector plot of 0.005m radius (left) and 0.045m radius (right)

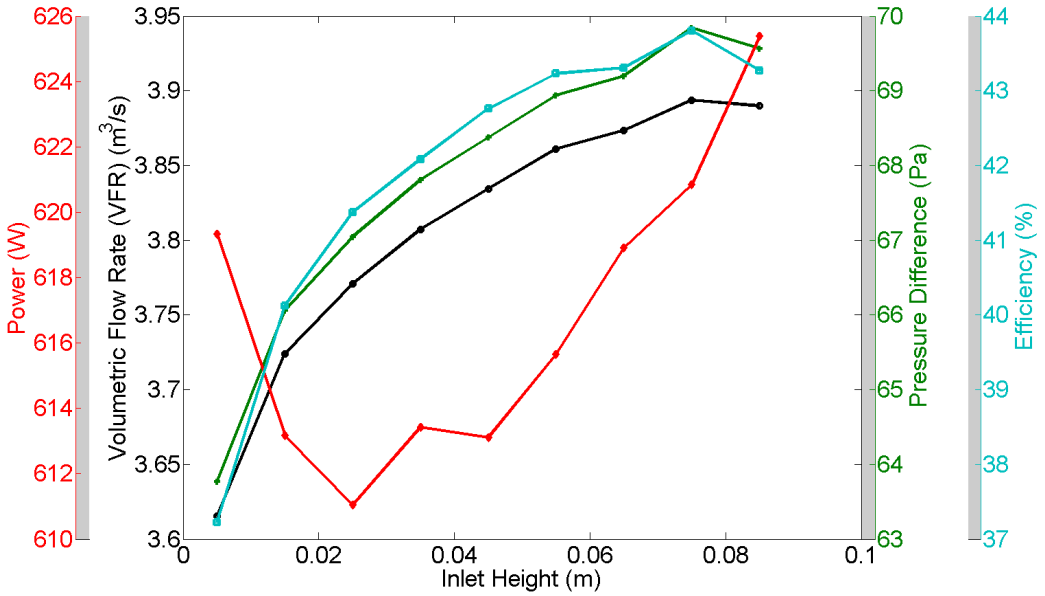

Figure 5.10: Changing inlet height with a constant 0.045m width

a maximum of 1.1%.

Again, the velocity distortion into the fan area is greater with a smaller inlet height, seen in Figure 5.11. Separation occurs in the fan region as well. The fast transition into the fan region does not allow the flow to straighten as it enters the fan

area as the larger heights with slower transitions allow.

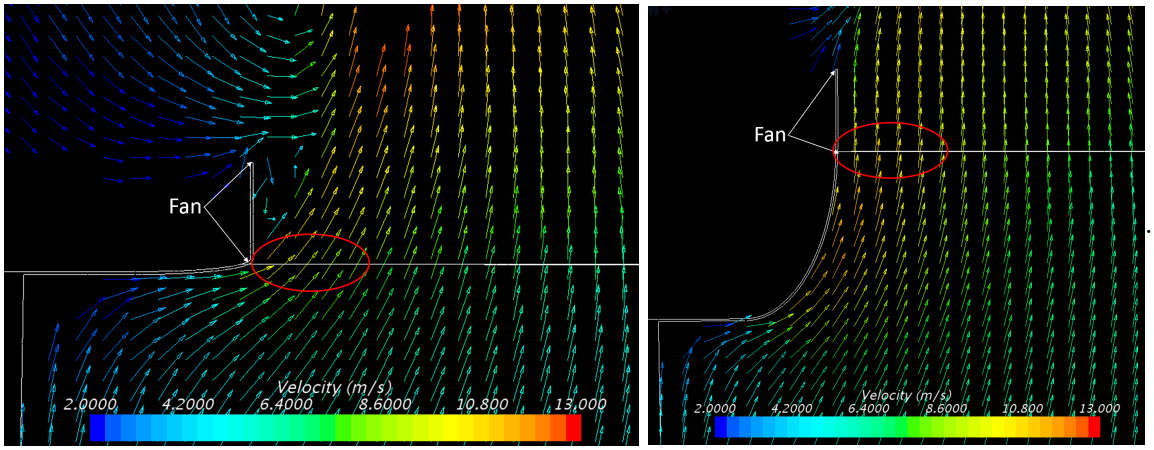

Figure 5.11: Velocity vector plot of 0.005m height (left) and 0.085m height (right)

The two variables, inlet width and height, both affect the flow dynamics, and therefore, examining their effects simultaneously is desired. The RSM detailed in Chapter 2 was used to analyze the responses from the two variable inputs of height and width. Using the VFR as the response variable, and the 18 combinations of the width and height as the two factor inputs, the resulting RSM equation is given by,

$$VFR = 3.56 + 3.55D + 7.37H - 56.69D^2 - 48.30DH + 0.99H^2 \qquad (5.1)$$

with a maximum VFR occurring at $D = 0.032$m and $H = 0.077$m.

The surface represented by this fitting is shown in Figure 5.12 with the individual data points used in the data fitting.

The data fitting and surface help show the trends that occur with changes across both factors. It is seen that the VFR increases with both larger widths and heights of the orifice. Increasing both factors provides a smoother transition at both the bottom and top of the orifice. The effects of a fast transition at the bottom of the orifice can be seen when comparing the velocity vector plot and the inflow distortions of the

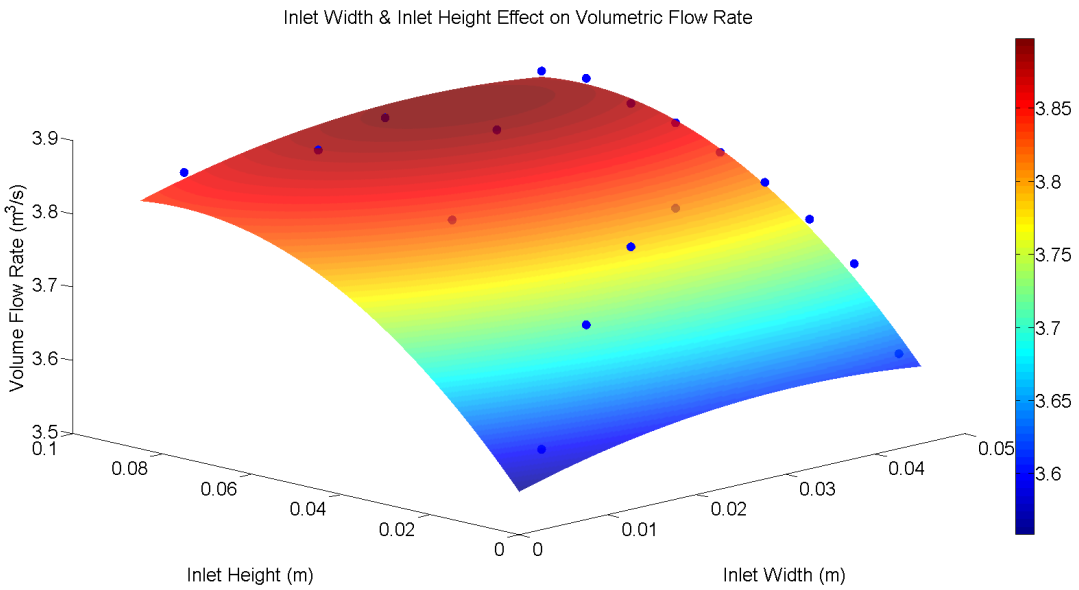

Figure 5.12: RSM surface plot with VFR response variable

$D = 0.005$m and $H = 0.085$m with the $D = 0.045$m and $H = 0.085$m simulation. As shown in Figure 5.13, the fast transition of $D = 0.005$m and $H = 0.085$m generates stronger velocity inflow distortions leading into the fan, and creates separation and back flow into the fan region, and reduces the overall VFR.

As VFR increases, so does the velocity of the flow through the condenser unit, resulting in better heat transfer on the coil. However, the highest VFR may not be the best overall fan efficiency of the unit as a whole if the fan performance is dramatically reduced. Therefore, the fan efficiency was also used as a response variable, and the resulting RSM fitting equation was,

$$\eta = 36.06 + 98.50D + 176.90H - 1701.57D^2 - 1360.96DH + 282.17H^2 \qquad (5.2)$$

with a maximum fan efficiency occurring at $D = 0.0346$m and $H = 0.0686$m. The surface given by this equation is shown in Figures 5.14.

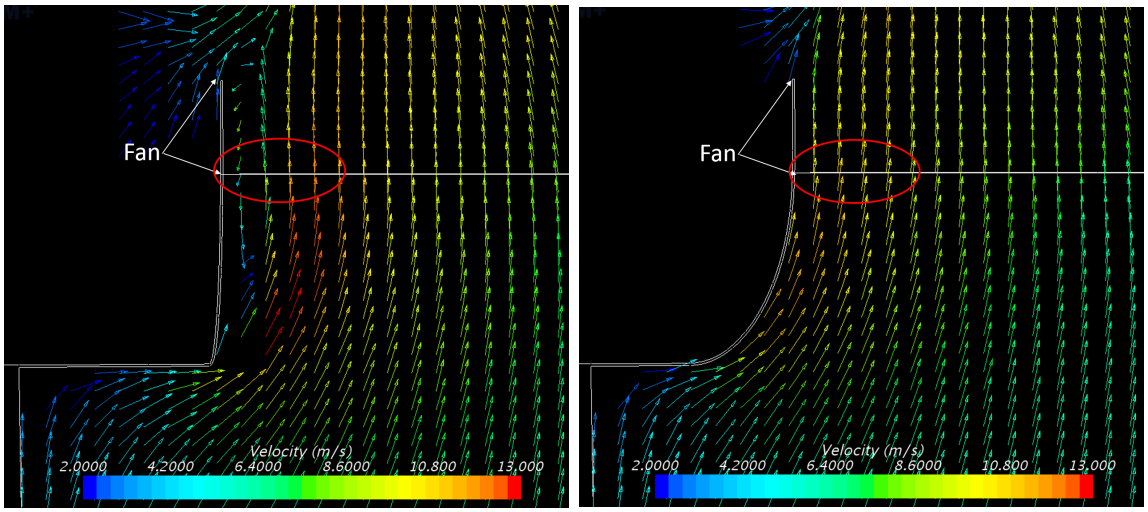

Figure 5.13: Velocity vector plot of 0.005m width (left) and 0.045m width (right) with same 0.085m height

The surface fit is similar to the VFR fit, with large initial gains in fan efficiency as the height is increased. The surface indicates a steeper drop in fan efficiency for small widths due to the large amount of off angle velocities entering the fan region at the sharper corners such as Figure 5.13.

Using the RSM equations, the two conditions resulting in a maximum response for VFR and fan efficiency were simulated in Star-CCM+® with the factors shown in Table 5.1.

Table 5.1: Simulation parameters for CFD model

Orifice Type	Width (m)	Height (m)	VFR (m^3/s)	Fan Efficiency (%)
Current	0.027	0.025	3.7886	41.63
VFR Optimal	0.0346	0.0686	3.8849	43.62
η Optimal	0.0320	0.0767	3.8841	43.63

The optimum orifice for VFR resulted in a volumetric flow rate of 3.8849 m^3/s

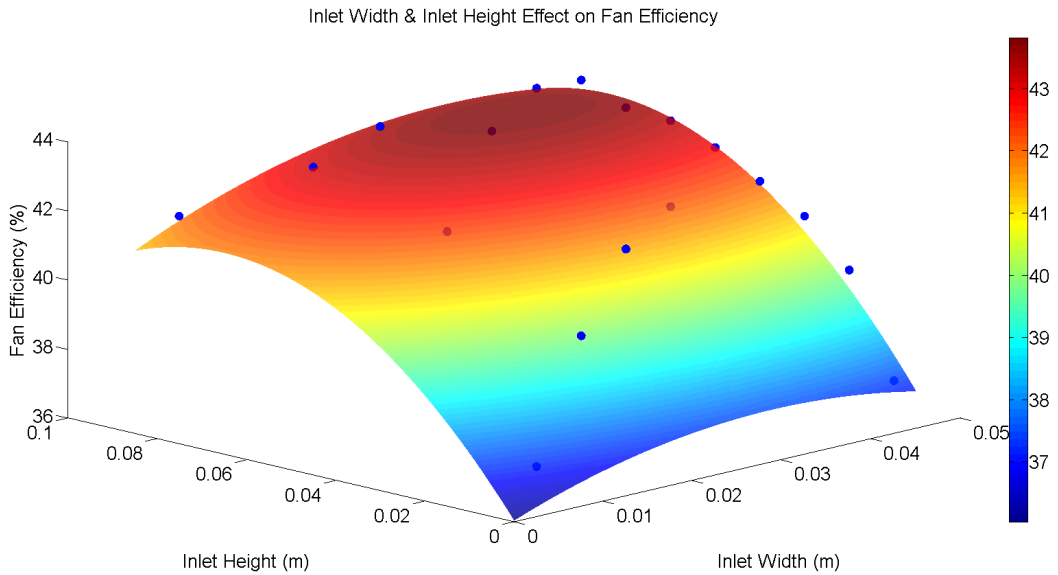

Figure 5.14: RSM surface plot with fan efficiency response variable

which was 0.31% under the predicted value of 3.897 m^3/s. The increase in the VFR over the original orifice can again be seen in the reduced inflow distortions (Figure 5.15) by providing a smooth transition into the fan. The optimal VFR orifice increased the VFR by 2.54% over the original orifice which produced a VFR of 3.7886 m^3/s.

The optimum orifice for increasing fan efficiency resulted in a 43.63% fan efficiency, which was 0.41% under the predicted value of 43.81%. Similar to the optimal VFR orifice, the optimal fan efficiency orifice creates a straighter flow into the fan region, as shown in Figure 5.16. These results show that the RSM can help show general trends within this region of the flow, and how the inlet geometry affects the response of interest.

Beyond the orifice helping with fan efficiency and total VFR increases, other areas of the flow could be targeted to help increase the fan efficiency on the overall condenser unit. As the flow becomes more turbulent upstream of the fan, the fan experiences drops in fan efficiency. Looking at the flow within the condenser, there

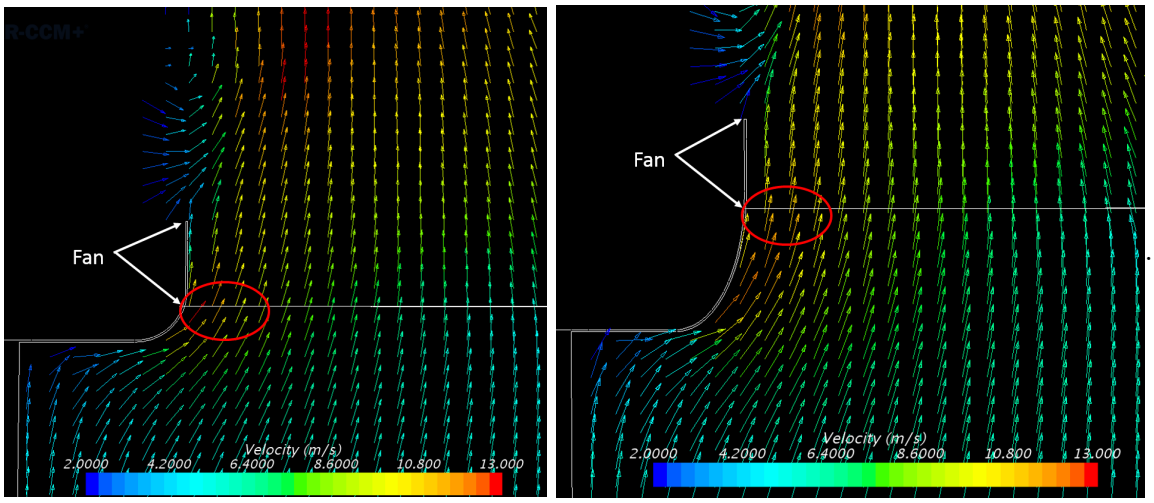

Figure 5.15: Velocity vector plot of original orifice (left) and VFR optimal orifice (right)

is turbulence created by the the coil not reaching entirely across the walls of the condenser unit. The TKE shows this generation at the inlet, seen in Figure 5.17, which propagates through to the fan as shown with the isosurface of TKE in Figure 5.18. Neither of the optimal orifices affect this region of flow, and continues to exist in the more efficient geometries.

The velocity distribution also contributes to overall condenser fan efficiency. To look at this distribution, the grid shown in Figure 4.2 was used to collect velocity data. A surface plot of the distribution was made and is shown in Figure 5.19. Looking at a side view of the surface plot for the original orifice and the VFR optimum orifice, the magnitude on the surface of the coil is increased for the optimum orifice (Figure 5.20), which results in better heat transfer rates and condenser fan efficiency. When the surface plot is normalized by the maximum velocity on the coil, however, the overall distribution remains unchanged from the original orifice to the optimum orifice (Figure 5.21). This distribution is driven by the characteristics of the coil, detailed in Chapter 4, and the fans ability to create a low pressure region within the unit,

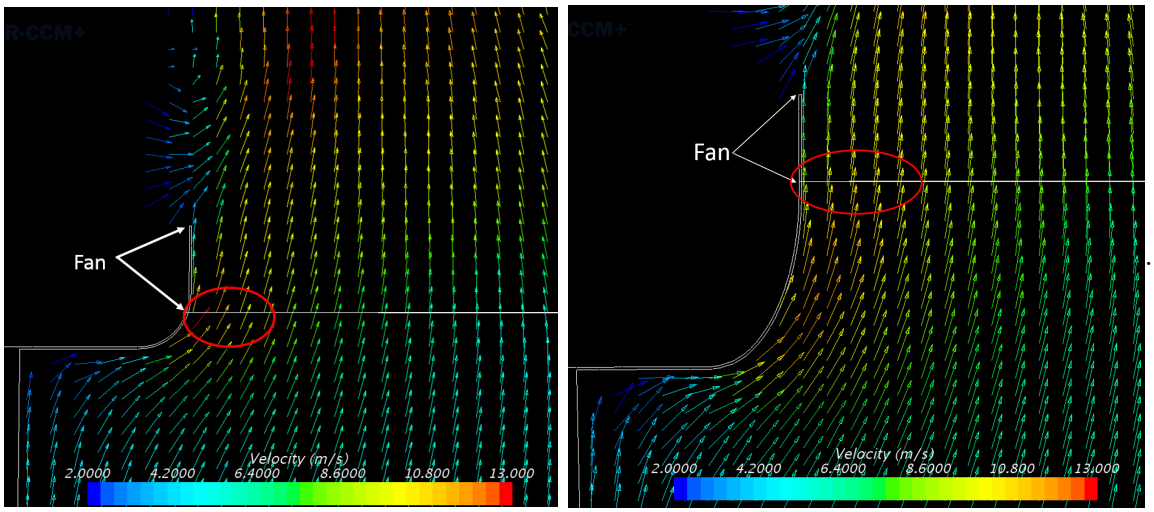

Figure 5.16: Velocity vector plot of original orifice (left) and fan efficiency optimal orifice (right)

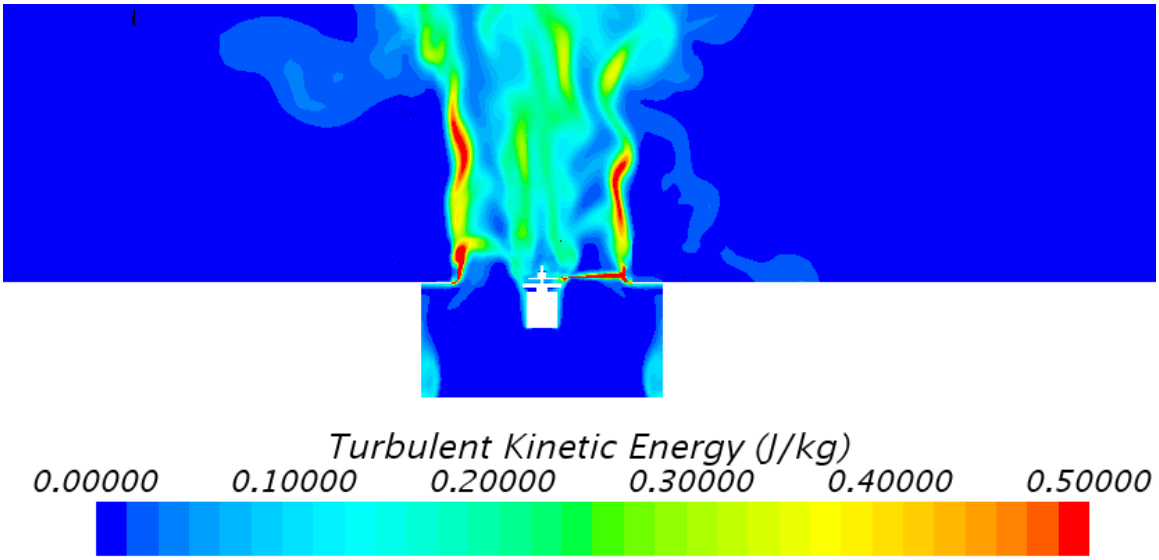

Figure 5.17: Front view of turbulent kinetic energy generation

drawing high pressure ambient air through the coil. The lowest pressure within the unit is just below the fan, and slowly increases through the unit as shown in Figure 5.22. Therefore, the largest differential pressure and highest velocity is at the top of the unit. This distribution could be changed by bringing the coil more horizontal.

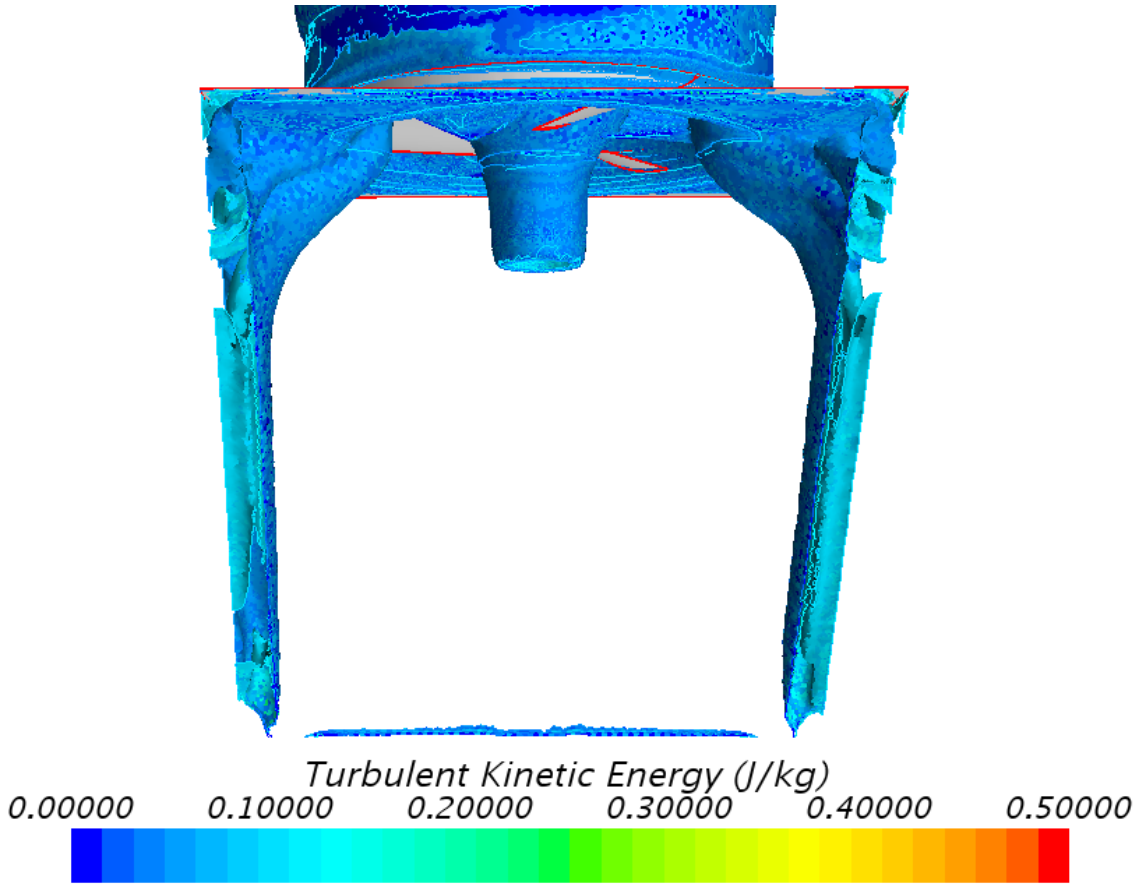

Figure 5.18: Isosurface of turbulent kinetic energy entering fan area

This would bring the distance from the coil to the fan, more uniform across the coil, causing similar pressure and velocity distributions on the coil.

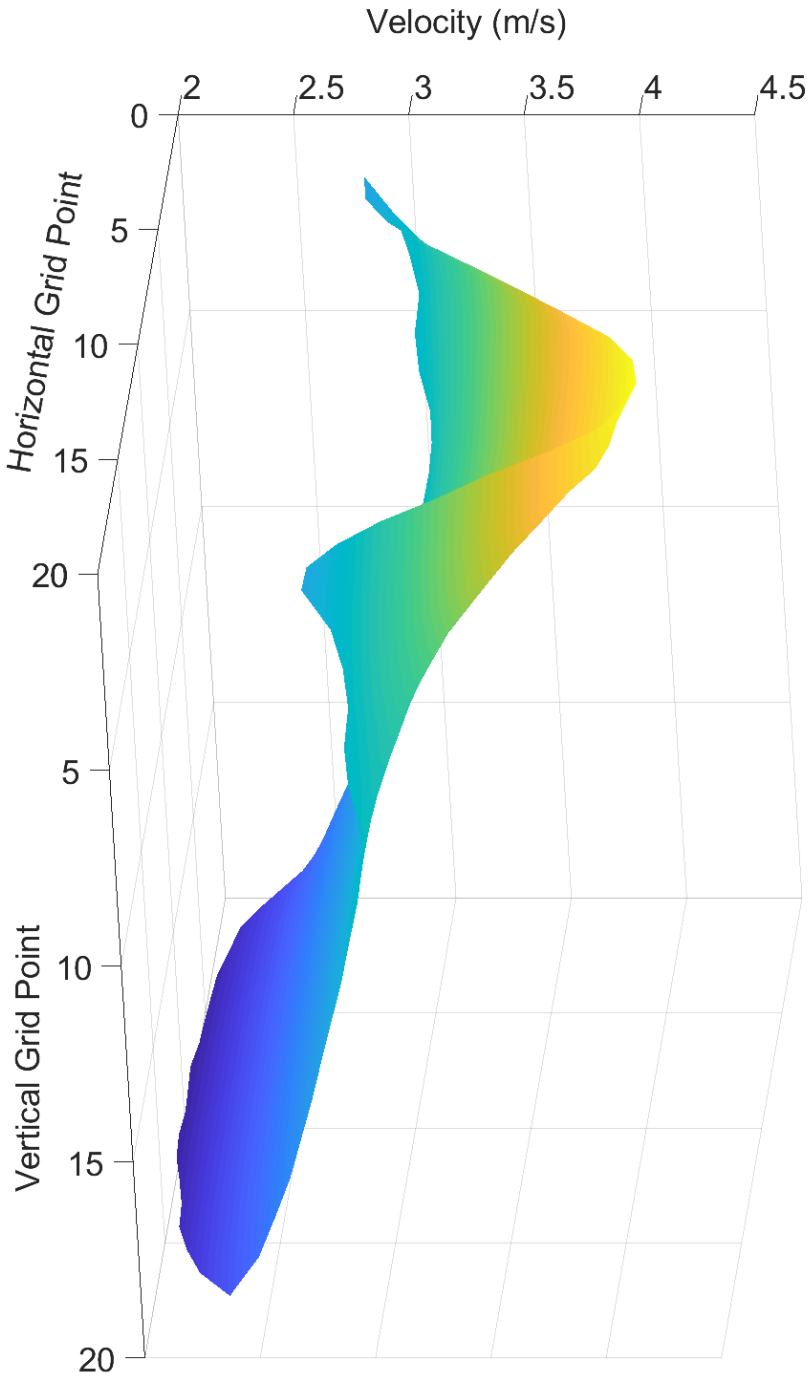

Figure 5.19: Surface plot of velocity distribution at the coil face

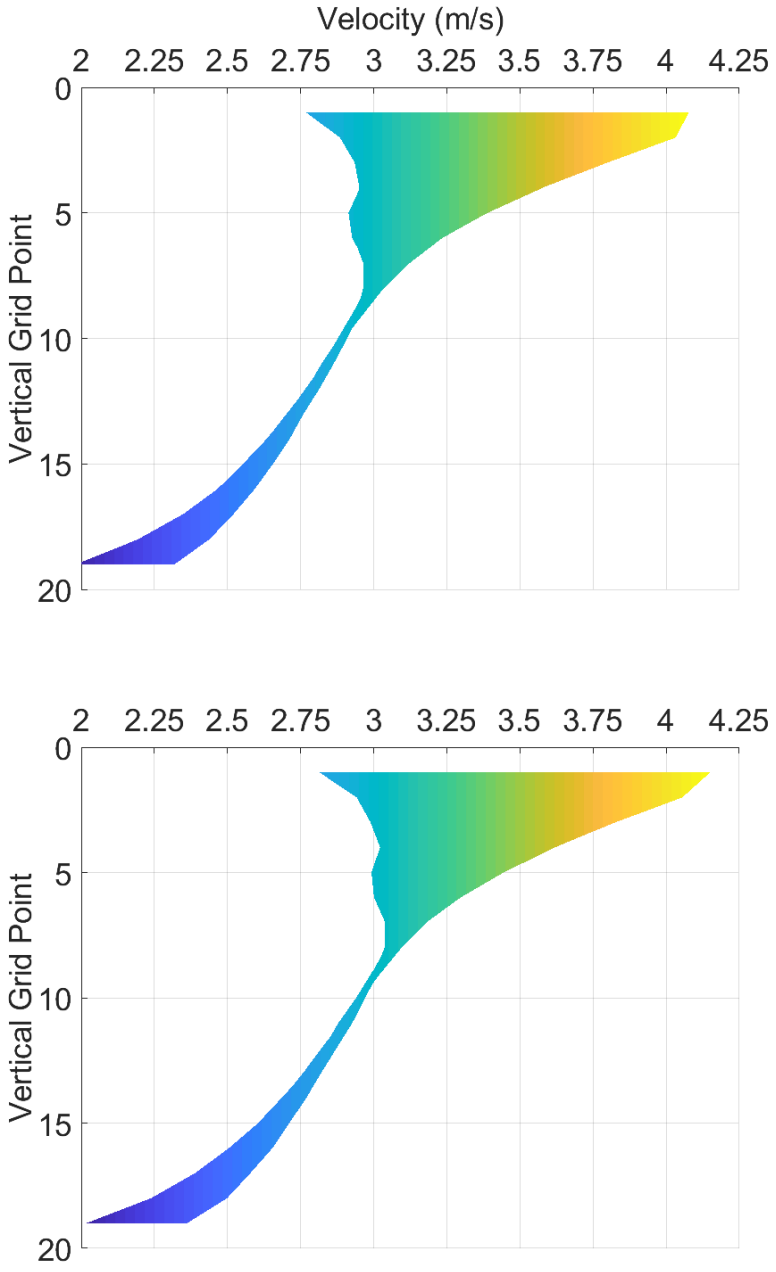

Figure 5.20: Magnitude comparison of velocity distribution at the face of the coil for original orifice (top) and most efficient orifice (bottom)

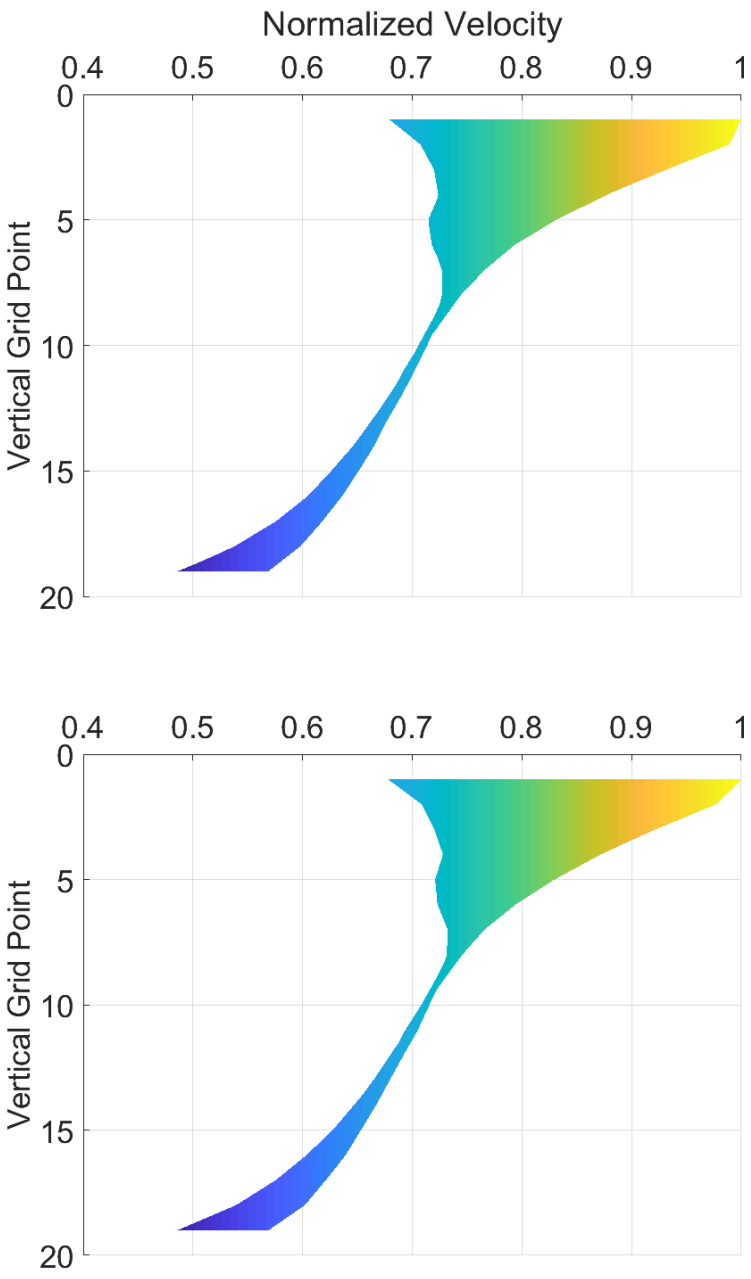

Figure 5.21: Normalized velocity distribution at the face of the coil for original orifice (top) and most efficient orifice (bottom)

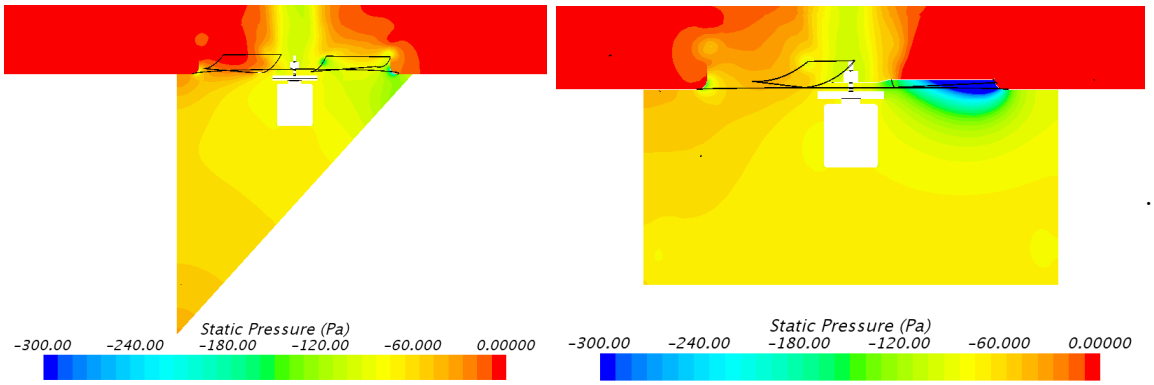

Figure 5.22: Pressure distribution upstream of fan driving flow velocity

Outlet Curvature

The effects of the outlet geometry changes are more complex than the inlet geometry changes, and is apparent by looking at the RSM fit shown in Figure 5.23. The surface does not well define the data, with many points lying well off the surface. Therefore, the RSM fit could not be used for analyzing the effects of the outlet geometry.

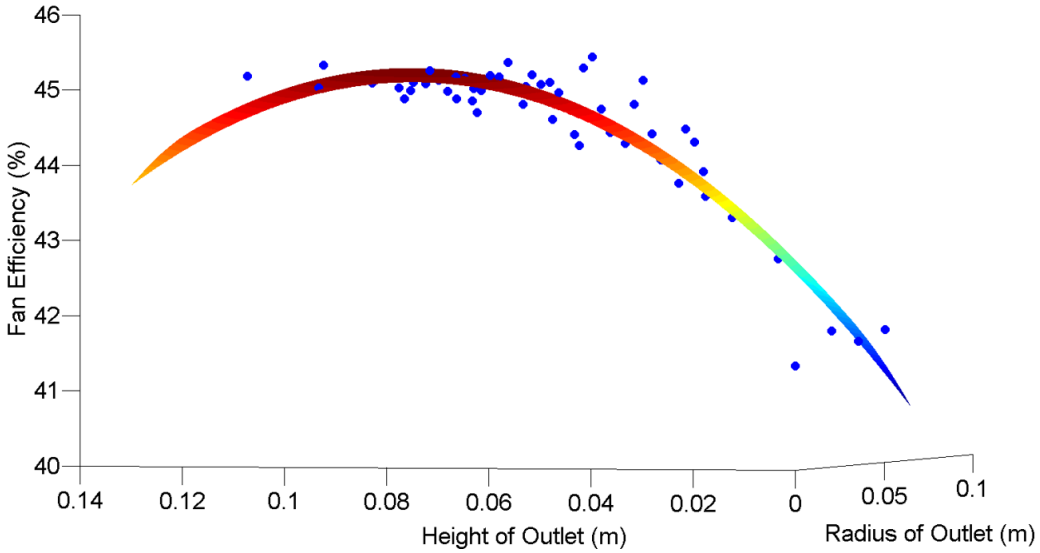

Figure 5.23: VFR response with increasing height for given width

A number of widths values were held constant while increasing the height. As the height increased, the VFR and fan efficiency both rose sharply and then began to plateau as shown in Figures 5.24 and 5.25.

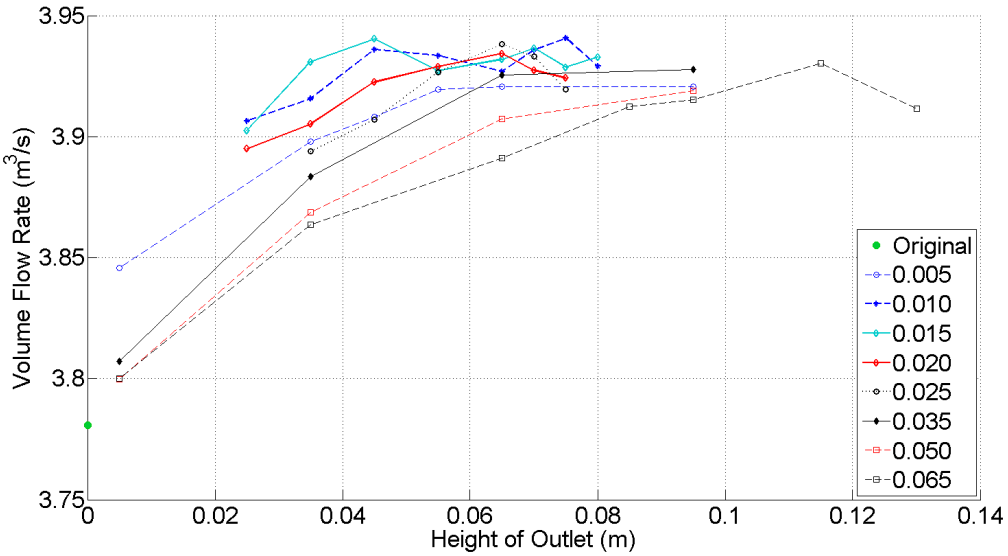

Figure 5.24: VFR response with increasing height for given width

Some maximum was reached for each radius that was studied, and then the trend stayed relatively flat. This suggests that increasing the height does not continually increase VFR and fan efficiency, and for any given radius of the outlet geometry, the height should only be increased to a certain value before there is no added benefit of further increases. This value can be correlated to the curvature nearest to the fan, calculated as,

$$\kappa = \frac{H^2}{D} \tag{5.3}$$

where κ is the curvature, and H and D are the vertical and horizontal radii of the orifice geometry, respectively.

Plotting the curvature and the fan efficiency, as seen in Figure 5.26, there is a sharp increase in fan efficiency by increasing the curvature. However, increasing the

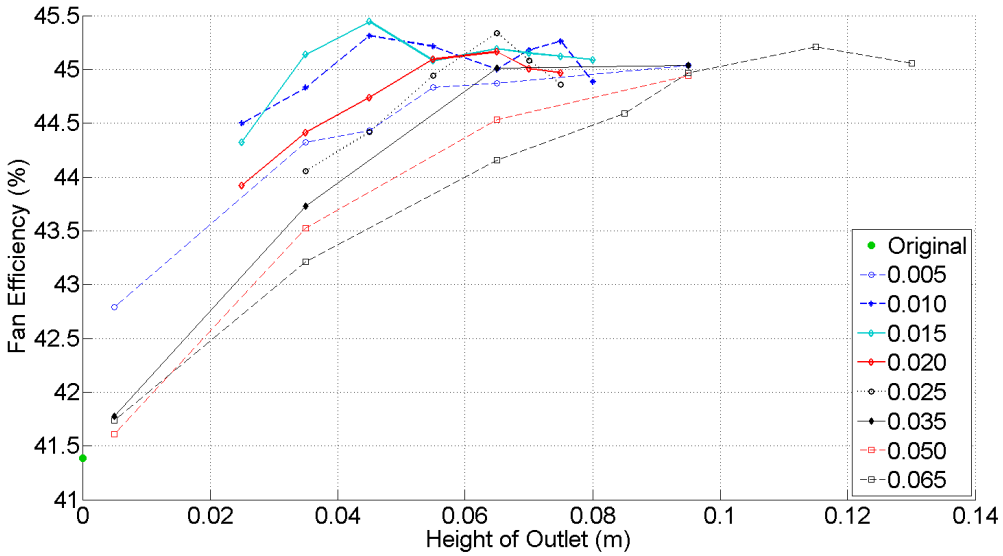

Figure 5.25: Efficiency response with increasing height for given width

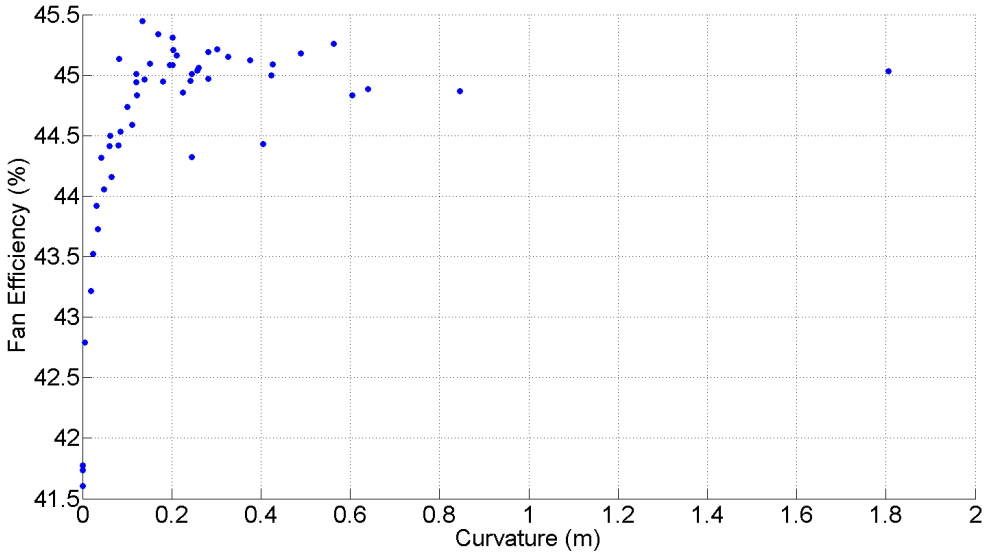

Figure 5.26: Efficiency distribution for curvature of outlet in the near fan region

curvature beyond 0.2m does not increase fan efficiency any further. The most efficient outlet curvature ocurred at D =0.015m and H =0.045m with a curvature of 0.135, which increased fan efficiency by 9.8% and VFR by 4.22%.

As the width of the outlet increases, the height must significantly increase much greater in order to achieve a curvature around 0.2m. Therefore, the maximum fan efficiency for each width, occurs further along the height. This is seen for a width of 0.065m, where a height of 0.114m must be used to have a 0.2m curvature. The simulation which gave the maximum response for this width occurred at 0.115m, adhering to the trend of no additional increase in fan efficiency beyond a curvature of 0.2m. This trend of the maximum occurring at a further increasing height for a given width can be seen in Figure 5.27, which shows an interpolated fit of the data, and a top view of the surface.

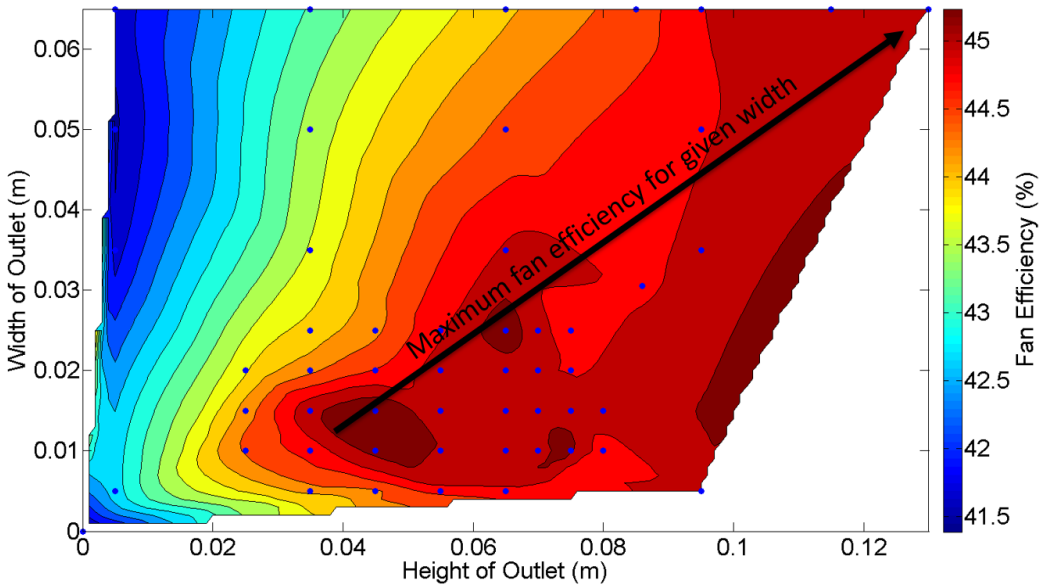

Figure 5.27: Interpolated fan efficiency response distribution with maximum fan efficiency trend

To understand how the outlet curvature helped increase VFR and fan efficiency, the pressure and vorticity at the outlet was studied. At the outlet, there is a fast change in pressure by discharging to a zero pressure, atmospheric condition. Such fast changes create large pressure gradients at the outlet, which lead to increased

flow distortions as the flow attempts to equalize the pressure gradient. The outlet curvature helps to decrease the pressure gradient, by providing a more gradual transition between the low and high pressure zone. By doing so, there is less flow distortion, which consumes energy, thus, increasing VFR and fan efficiency. The strong pressure gradient that exists for the original orifice is largely dissipated by the D =0.015m, H =0.045m orifice as shown in Figure 5.28. The pressure gradient contributes to a large amount of vorticity with the original orifice (Figure 5.29) which decreases the overall VFR and fan efficiency. If the curvature of the outlet is extended

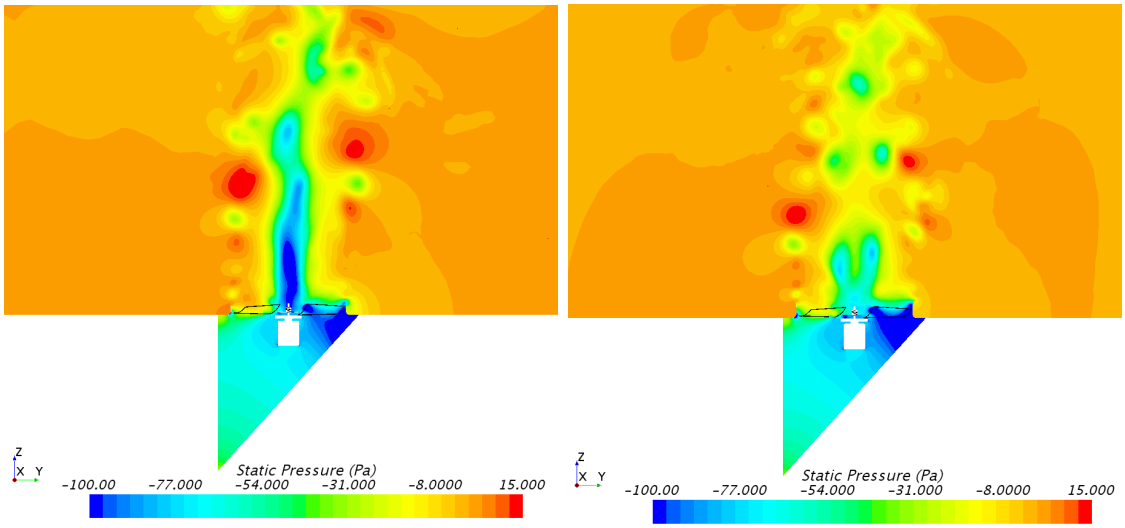

Figure 5.28: Pressure of original orifice (left) and most efficient outlet orifice (right)

beyond the optimal curvature, the height is extended much further without increasing the width. This results in an extended, almost straight, section followed by a quick transition to atmospheric condition. This type of outlet provides a strong pressure gradient since the final transition is still rather sudden, and produces an inefficient flow. This can be seen in Figure 5.30, where the D =0.015m orifice is extended past its optimal radius of 0.045m to 0.075m.

Looking at the velocity profile on the surface of the coil, there is again an increase

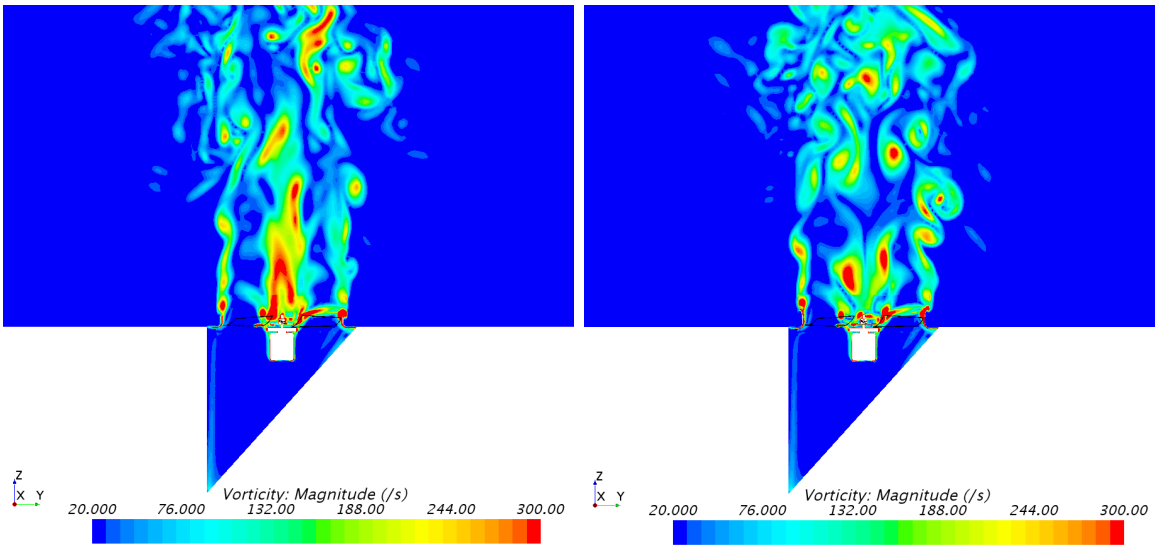

Figure 5.29: Vorticity of original orifice (left) and most efficient outlet orifice (right)

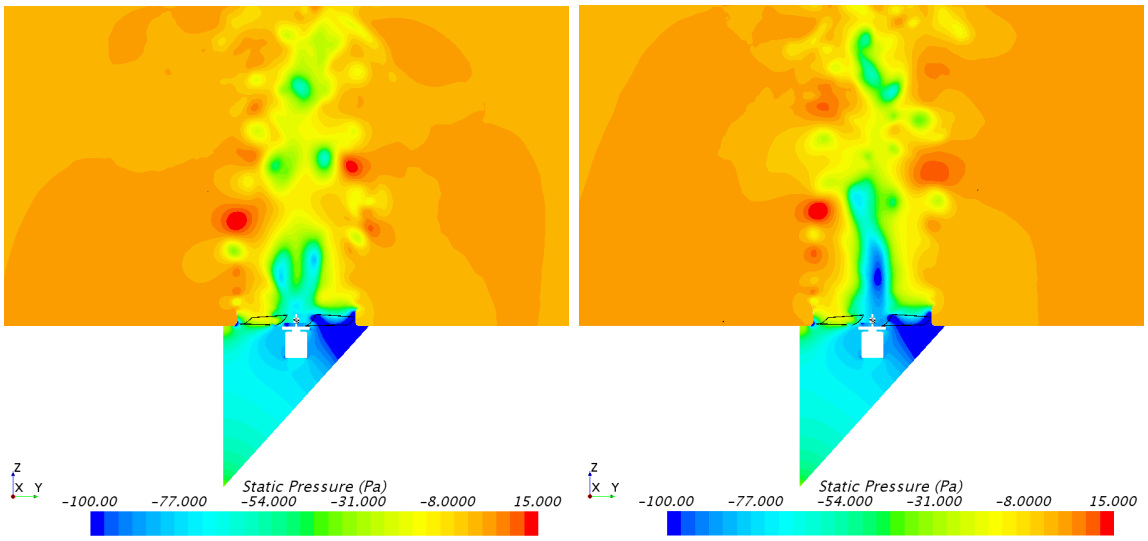

Figure 5.30: Pressure of most efficient orifice (left) and orifice with increased curvature beyond optimal (right)

when the magnitude of the highest fan efficiency outlet is compared to the original orifice (Figure 5.31). However, when normalized, the distribution is the same, showing that the outlet, like the inlet, does not help to increase heat transfer fan efficiency of the coil by providing a better distribution on the coil (Figure 5.32).

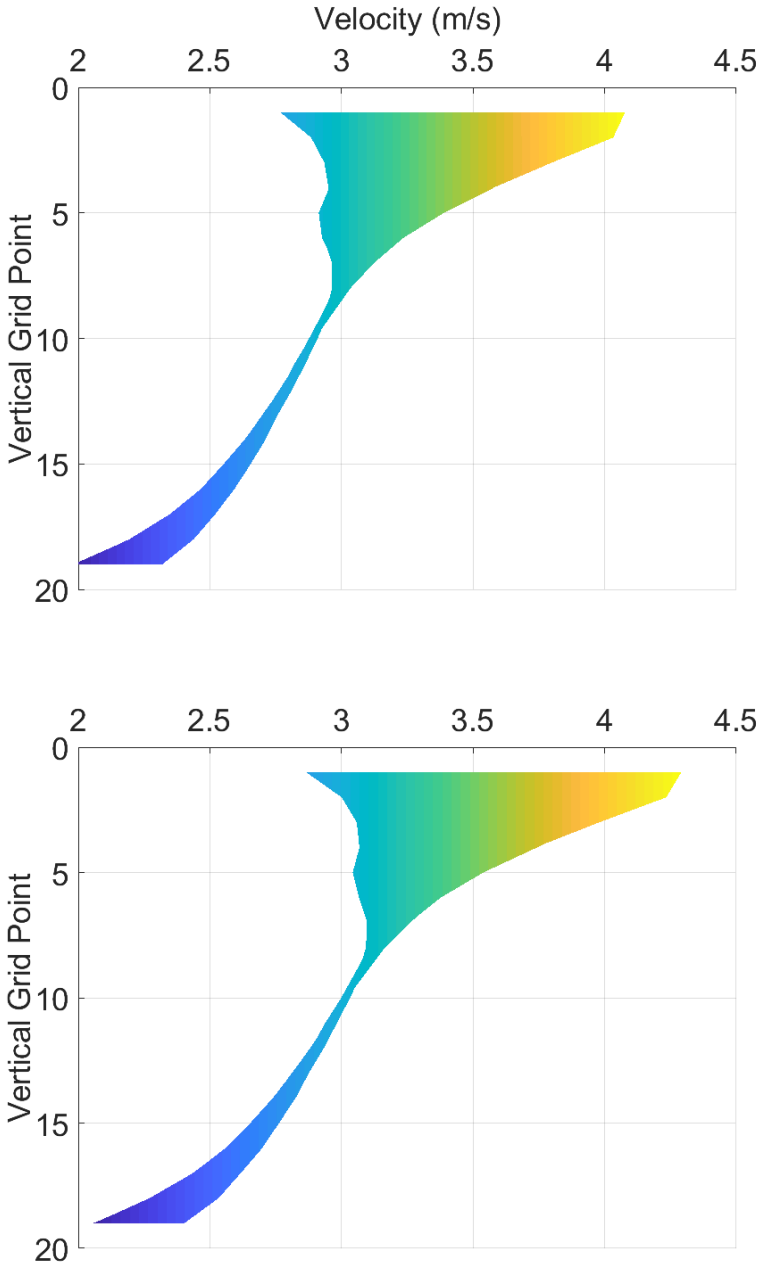

Figure 5.31: Magnitude comparison of velocity distribution at the face of the coil for original orifice (top) and most efficient orifice (bottom)

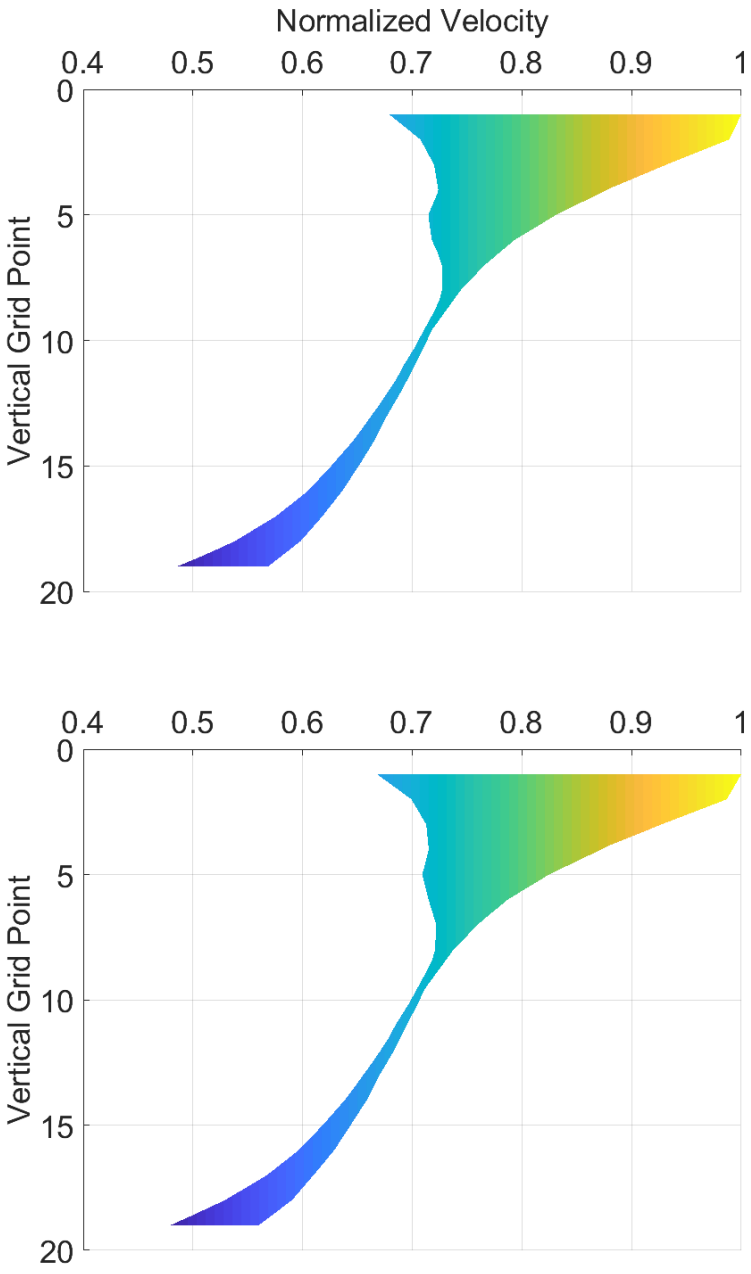

Figure 5.32: Normalized velocity distribution at the face of the coil for original orifice (top) and most efficient orifice (bottom)

Combined Orifice

The inlet curvature and outlet curvature increase the overall VFR and fan efficiency through different mechanisms. The inlet curvature provides a smoother and more consistent flow into the fan region, which helps increase the performance of the fan. Whereas, the outlet helps provide a smaller pressure gradient at the outlet as the flow changes from a low to a high pressure region. By reducing this pressure gradient, there is less resistance in the flow, and less energy spent on creating turbulence. Therefore, since the inlet and outlet affect different regions of the flow through different mechanics, changing both the inlet and outlet simultaneously, should increase the flow VFR and fan efficiency beyond the maximum when only one were changed.

A redesigned orifice used the highest performing inlet and outlet sections and was simulated in CFD. The resulting orifice produced a VFR of $4.056 m^3/s$ or a 7.05% increase in over the original orifice, and an fan efficiency of 48.23%, from the original orifice at 41.63%. The decreased vorticity in the two separate regions can be seen in Figures 5.33 and 5.34. This show that the two regions do increase fan efficiency due to different mechanics, and using both regions together provides a much higher increase in VFR and fan efficiency.

The results for VFR and fan efficiency for the original, and all optimal cases are shown in Table 5.2.

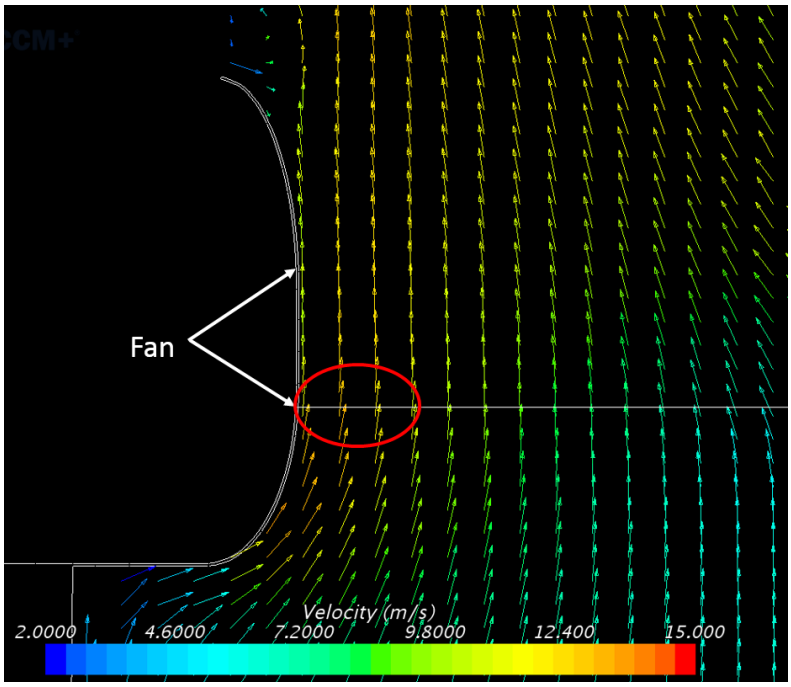

Figure 5.33: Velocity vector plot at inlet of combined orifice

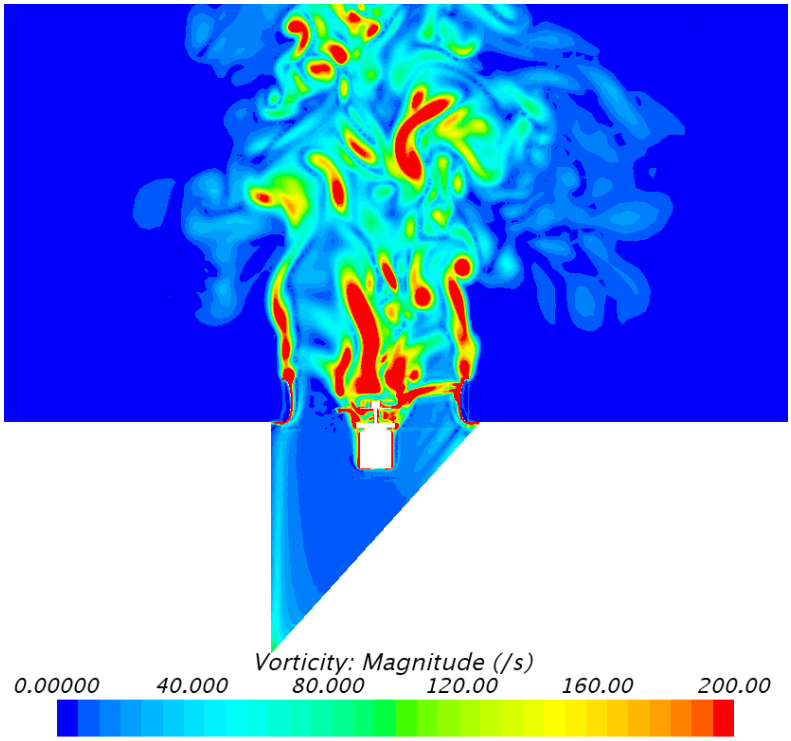

Figure 5.34: Vorticity at outlet of combined orifice

Table 5.2: Simulation results for optimal designs

Simulation	VFR (m^3/s)	VFR Increase(%)	Fan Efficiency (%)	Fan Efficiency Increase (%)
Current	3.7886	NA	41.63	NA
Inlet (η optimal)	3.8841	2.52	43.63	4.8
Outlet	3.9404	4.01	45.44	9.16
Combined	4.0555	7.05	48.23	15.85

CHAPTER SIX

CONCLUSION

This research aimed to redesign the orifice plate surrounding the axial fan of an air-cooled condenser unit using CFD in the design process. Using CFD to analyze design iterations, eliminated the need to physically build time consuming and expensive prototypes for each design. By reducing this time cost, more design changes can be iterated in order to converge on an optimal design. CFD can also be used to visualize and analyze regions of the flow that are difficult to obtain with physical experiments. A CFD simulation used a porous region inlet to model the cooling coil, eliminating the need to create complicated and computationally expensive geometries. Experimental data was used to calibrate the physics of the coil within the simulation, by providing inertial and viscous resistance coefficients to the CFD program. An unsteady, detached eddy simulation was then used to run the model for 27.5 rotations of the fan, allowing all parameters of interest to converge. The CFD simulation was first validated with experimental data in order to ensure that the model was capturing the general physics of the real-world flow.

Velocity data was collected experimentally from the unit by traversing an air velocity meter from the center of the fan outward, for three separate azimuthal locations. Additionally, for each location three vertical positions of the traverse were performed. In the CFD simulation, line probes were placed at the same collection point of the physical experiments. A direct comparison of the experimental and simulation data was difficult due to the air velocity meter probe, and its ability to be influenced by x and y components of the velocity. However, the z-component velocity data was time-averaged and compared to the experimental data. There was

good agreement between the experimental and simulation data, with the experimental values slightly above the simulation values. This was in part due to the additional x and y velocity components felt by the probe. The trends between the two data sets matched well for all locations and vertical positions within the flow. After validating the CFD model, the same simulation was used to redesign the orifice.

First, the inlet region of the orifice, which affects the flow upstream of the fan was studied. In this region, the geometry was changed by varying the minor and major radii of a quarter ellipse. For a given horizontal radius of the ellipse, it was found that as the vertical radius increased, there was an initial sharp increase in both volume flow rate and fan efficiency. However, as the vertical radius was increased, the VFR and fan efficiency plateaued before decreasing. This suggested that there was some optimal combination for the horizontal and vertical radii. This optimal design was found using a rough surface method to find an optimal response over a multi-variable space. Using this method, the fan efficiency was increased by 4.8% using the optimal dimensions. This increase in fan efficiency was due to the decreased vorticity directly upstream of the fan, allowing the fan to operate more effectively.

The outlet region of the orifice was then studied using the same quarter ellipse geometry, and varying the horizontal and vertical radii. In this region, there is a large pressure gradient from the fan discharging to atmospheric conditions. Providing a better transition and smaller pressure gradients, the performance of the flow was improved. In this outlet region it was found that the optimal geometry was correlated to curvature just downstream of the fan. Increasing curvature beyond 0.2m, and therefore creating a longer and straighter outlet, resulted in no additional increase in fan efficiency. The best simulated outlet improved VFR and η by 4.01% and 9.16%, respectively.

Since the two regions were improving different parts of the flow, it was predicted

that combining both regions into a new design would allow increases in both regions to continue independently, resulting in an even higher fan efficiency. The combined orifice resulted in a VFR and fan efficiency increase of 7.05% and 15.85%, respectively, confirming that the two geometry regions increase fan efficiency differently.

Though the design process resulted in an improved orifice plate that will help improve condenser fan efficiency, the research presented in this thesis could be expanded in a number of ways to further increase the overall effectiveness of the condenser unit. Improving the flow distribution on the coil face is one area that could be investigated. The distribution could be improved by changing the angle the coil is held at within the unit, or the overall shape and size of the coil. Providing a more uniform distribution would create better heat transfer, and potentially provide more uniform flow to the fan as well, improving the overall unit.

REFERENCES CITED

[1] "How much energy is consumed in U.S. residential and commercial buildings? - FAQ - U.S. Energy Information Administration (EIA)."

[2] "Residential Energy Consumption Survey (RECS) - Data - U.S. Energy Information Administration (EIA)."

[3] "CBECS 2012: Energy Usage Summary."

[4] K. J. Chua, S. K. Chou, W. M. Yang, and J. Yan, "Achieving better energy-efficient air conditioning A review of technologies and strategies," vol. 104, pp. 87–104.

[5] G. Ma and X. Li, "Exergetic optimization of a key design parameter in heat pump systems with economizer coupled with scroll compressor," vol. 48, no. 4, pp. 1150–1159.

[6] L. Zhang, C. Dang, and E. Hihara, "Performance analysis of a no-frost hybrid air conditioning system with integrated liquid desiccant dehumidification," vol. 33, no. 1, pp. 116–124.

[7] Z. Sun, S. Wang, and Z. Ma, "In-situ implementation and validation of a CO2-based adaptive demand-controlled ventilation strategy in a multi-zone office building," vol. 46, no. 1, pp. 124–133.

[8] T. Akimoto, S.-i. Tanabe, T. Yanai, and M. Sasaki, "Thermal comfort and productivity - Evaluation of workplace environment in a task conditioned office," vol. 45, no. 1, pp. 45–50.

[9] N/A, *2013 ASHRAE Handbook - Fundamentals*. American Society of Heating, Refrigerating and Air-Conditioning Engineers, Inc.

[10] B. P. Rao, B. Sunden, and S. K. Das, "An Experimental and Theoretical Investigation of the Effect of Flow Maldistribution on the Thermal Performance of Plate Heat Exchangers," vol. 127, no. 3, pp. 332–343.

[11] J. Moore, R. Grimes, and E. Walsh, "Influence of the Flow From an Axial Fan on the Performance of a Heat Exchanger," no. 54969, pp. 129–138.

[12] J. Hurault, S. Kouidri, F. Bakir, and R. Rey, "Experimental and numerical study of the sweep effect on three-dimensional flow downstream of axial flow fans," vol. 21, no. 2, pp. 155 – 165.

[13] L. Zhang and Y. Z. Jin, "Effect of Blade Numbers on Aerodynamic Performance and Noise of Small Axial Flow Fan," vol. 199-200, pp. 796–800.

[14] M. Milavec, B. irok, D. V. de Ventos, and M. Hoevar, "Influence of the shape of the blade tip on the emitted noise in the air-gap between the rotor and the housing of an axial faneinfluss des fluegelgipfelprofils auf dem abgestrahlten schallpegel im bereich der luftspalte zwischen rotor und stator eines axialventilators," vol. 78, no. 3-4, pp. 107–119.

[15] F. Kameier and W. Neise, "Experimental Study of Tip Clearance Losses and Noise in Axial Turbomachines and Their Reduction," vol. 119, no. 3, pp. 460–471.

[16] T. Fukano, Y. Takamatsu, and Y. Kodama, "The effects of tip clearance on the noise of low pressure axial and mixed flow fans," vol. 105, no. 2, pp. 291 – 308.

[17] A. Guedel, M. Robitu, and V. Chaulet, "Energy Efficiency of an Axial Fan for Various Casing Configurations," vol. 135, no. 7, p. 074501.

[18] P. Liu, N. Shiomi, Y. Kinoue, T. Setoguchi, and Y.-z. Jin, "Effect of Inlet Geometry on Fan Performance and Inlet Flow Fields in a Semi-opened Axial Fan," vol. 7, no. 2, pp. 60–67.

[19] G. Ren, S. Heo, T.-H. Kim, and C. Cheong, "Response surface method-based optimization of the shroud of an axial cooling fan for high performance and low noise," vol. 27, no. 1, pp. 33–42.

[20] H. Wang, J. Tian, H. Ouyang, Y. Wu, and Z. Du, "Aerodynamic performance improvement of up-flow outdoor unit of air conditioner by redesigning the bell-mouth profile," vol. 46, pp. 173–184.

[21] Z. Sun and S. Wang, "A CFD-based test method for control of indoor environment and space ventilation," vol. 45, no. 6, pp. 1441–1447.

[22] W. Yaci, M. Ghorab, and E. Entchev, "Numerical analysis of heat and energy recovery ventilators performance based on CFD for detailed design," vol. 51, no. 1, pp. 770–780.

[23] M. J. Moran, H. N. Shapiro, D. D. Boettner, and M. B. Bailey, *Fundamentals of Engineering Thermodynamics*. John Wiley & Sons, 7th ed.

[24] R. C. Jordan and G. B. Priester, *Refrigeration and Air Conditioning*. Prentice Hall.

[25] R. American Society of Heating and I. Air-Conditioning Engineers, *2016 ASHRAE Handbook - Heating, Ventilating, and Air-Conditioning Systems and Equipment (SI Edition)*. American Society of Heating, Refrigerating and Air-Conditioning Engineers, Inc.

[26] "AAON Heating and Cooling Products."

[27] Z. Zhang, J. Yang, and Y. Wang, "A favorable face velocity distribution and a V-frame cell for power plant air-cooled condensers," vol. 87, pp. 1–9.

[28] K. Duvenhage, J. A. Vermeulen, C. J. Meyer, and D. G. Krger, "Flow distortions at the fan inlet of forced-draught air-cooled heat exchangers," vol. 16, no. 8, pp. 741–752.

[29] J. M. F. Oro, K. M. A. Daz, C. S. Morros, and E. B. Marigorta, "Analysis of the Deterministic Unsteady Flow in a Low-Speed Axial Fan With Inlet Guide Vanes," vol. 130, no. 3, pp. 031101–031101–12.

[30] J. Tu, G.-H. Yeoh, and C. Liu, *Computational Fluid Dynamics A Practical Approach*. Butterworth-Heinemann.

[31] M. A. Jemni, G. Kantchev, and M. S. Abid, "Influence of intake manifold design on in-cylinder flow and engine performances in a bus diesel engine converted to LPG gas fuelled, using CFD analyses and experimental investigations," vol. 36, no. 5, pp. 2701–2715.

[32] T. Tezdogan, Y. K. Demirel, P. Kellett, M. Khorasanchi, A. Incecik, and O. Turan, "Full-scale unsteady RANS CFD simulations of ship behaviour and performance in head seas due to slow steaming," vol. 97, pp. 186–206.

[33] N. Frink, S. Pirzadeh, J. Morrison, H. Atkins, S. Viken, and J. Morrison, "CFD assessment of aerodynamic degradation of a subsonic transport due to airframe damage," in *48th AIAA Aerospace Sciences Meeting Including the New Horizons Forum and Aerospace Exposition*, p. 500.

[34] Y. Li, K.-J. Paik, T. Xing, and P. M. Carrica, "Dynamic overset CFD simulations of wind turbine aerodynamics," vol. 37, no. 1, pp. 285–298.

[35] Y. Jiang and Q. Chen, "Study of natural ventilation in buildings by large eddy simulation," vol. 89, no. 13, pp. 1155–1178.

[36] R. Al-Waked, M. S. Nasif, G. Morrison, and M. Behnia, "CFD simulation of air to air enthalpy heat exchanger," vol. 74, pp. 377–385.

[37] F. Prot, M.-S. Kim, K. Wada, K. Norisada, M. Kitada, S. Hirayama, M. Sakai, S. Imahigasi, and N. Sasaki, "HVAC Blower Aeroacoustics Predictions Based on the Lattice Boltzmann Method," pp. 921–929.

[38] A. I. Khuri and J. A. Cornell, *Response Surfaces: Designs and Analyses: Second Edition*. CRC Press.